








A deeply conserved protease, acylamino acid-releasing enzyme (AARE), acts in ageing in *Physcomitrella* and *Arabidopsis*

Sebastian N. W. Hoernstein ¹, Buğra Özdemir^{1,5}, Nico van Gessel ¹, Alessandra A. Miniera¹, Bruno Rogalla von Bieberstein ^{1,6}, Lars Nilges¹, Joana Schweikert Farinha ^{1,7}, Ramona Komoll^{1,8}, Stella Glauz¹, Tim Weckerle^{1,9}, Friedrich Scherzinger ^{1,10}, Marta Rodriguez-Franco ², Stefanie J. Müller-Schüssele³ & Ralf Reski ^{1,4}✉

Reactive oxygen species (ROS) are constant by-products of aerobic life. In excess, ROS lead to cytotoxic protein aggregates, which are a hallmark of ageing in animals and linked to age-related pathologies in humans. Acylamino acid-releasing enzymes (AARE) are bifunctional serine proteases, acting on oxidized proteins. AARE are found in all domains of life, albeit under different names, such as acylpeptide hydrolase (APEH/ACPH), acylaminoacyl peptidase (AAP), or oxidized protein hydrolase (OPH). In humans, AARE malfunction is associated with age-related pathologies, while their function in plants is less clear. Here, we provide a detailed analysis of AARE genes in the plant lineage and an in-depth analysis of AARE localization and function in the moss *Physcomitrella* and the angiosperm *Arabidopsis*. AARE loss-of-function mutants have not been described for any organism so far. We generated and analysed such mutants and describe a connection between AARE function, aggregation of oxidized proteins and plant ageing, including accelerated developmental progression and reduced life span. Our findings complement similar findings in animals and humans, and suggest a unified concept of ageing may exist in different life forms.

¹Plant Biotechnology, Faculty of Biology, University of Freiburg, Schaezlestrasse 1, 79104 Freiburg, Germany. ²Cell Biology, Faculty of Biology, University of Freiburg, Schaezlestrasse 1, 79104 Freiburg, Germany. ³Molecular Botany, Department of Biology, Technical University of Kaiserslautern, Erwin-Schrödinger-Strasse 70, 67663 Kaiserslautern, Germany. ⁴Signalling Research Centres BIOS and CIBSS, Schaezlestrasse 18, 79104 Freiburg, Germany. ⁵Present address: Euro-Biolmaging Bio-Hub, EMBL Heidelberg, Meyerhofstraße 1, 69117 Heidelberg, Germany. ⁶Present address: Department of Anesthesiology, University Hospital Würzburg, Oberduerrbacher Strasse 6, 97072 Würzburg, Germany. ⁷Present address: Institute for Molecular Biosciences, Goethe University Frankfurt, Max-von-Laue-Str. 9, 60438 Frankfurt, Germany. ⁸Present address: Heraeus Medical GmbH, Philipp-Reis-Straße 8-13, 61273 Wehrheim, Germany. ⁹Present address: Zymo Research Europe GmbH, Muelhauser Strasse 9, 79110 Freiburg, Germany. ¹⁰Present address: Centre for Integrative Biodiversity Research (iDiv) Halle-Jena-Leipzig, Puschstrasse 4, 04103 Leipzig, Germany. ✉email: ralf.reski@biologie.uni-freiburg.de

Reactive oxygen species (ROS) are by-products of O_2 metabolism and represent a challenge to all aerobic life. ROS play a dual role as potentially lethal oxidants and as signaling molecules¹. Therefore, aerobic organisms possess sophisticated redox systems to scavenge and detoxify excess ROS. The major sources of ROS in plant cells are the electron transport chains in mitochondria and plastids, but also in peroxisomes and at the plasma membrane². Environmental stresses such as heat, drought, or intense light are factors for increasing ROS production to detrimental levels. Plants possess a repertoire of detoxifying enzymes such as catalases, superoxide dismutases, ascorbate peroxidases, glutathione peroxidase-like proteins, and peroxiredoxins. Electrons for reduction are largely provided via non-enzymatic components such as ascorbic acid, glutathione, and NADPH^{3–7}. In addition, a range of heat-shock proteins assist in disaggregation or refolding of damaged proteins^{8–10}.

Despite conversion into non-toxic derivatives, the continuous exposure to ROS results in oxidation of DNA, lipids, and proteins⁵. On the protein level, ROS lead to irreversible cysteine oxidation, advanced glycation end products, adducts with ROS-generated reactive aldehydes, and carbonylation of amino acid side-chains^{11,12}. If not cleared via proteolysis, an excess of oxidized proteins accumulates to cytotoxic protein aggregates. Plant antioxidant systems and the role of ROS as signaling molecules in abiotic stress responses are well studied¹³. Yet, factors involved in a plant cell's last line of defense, such as the proteolytic systems for the clearance of irreversibly oxidized proteins, are still underexplored.

A class of serine proteases is evolutionary deeply conserved as their activity is found in bacteria, archaea, animals and plants, and can degrade irreversibly oxidized proteins^{14–17}. These proteases have different names in different organisms, e.g. acylamino acid-releasing enzyme (AARE), acylpeptide hydrolase (APEH/ACPH), acylaminoacyl peptidase (AAP), or oxidized protein hydrolase (OPH)¹⁸ but are collectively addressed as AARE here. AARE acts in multimeric complexes^{14,17} as a bifunctional protease as it cleaves N^{α} -acetylated amino acids from oligopeptides via an exopeptidase mode, but also cleaves oxidized proteins via an endopeptidase mode^{16,19–22}. AARE isoforms from various organisms show different specificities towards N^{α} -acetylated amino acids, with bacterial and archaeal enzymes preferring AcLeu and AcPhe substrates^{15,23–25} and plant and animal isoforms preferring AcAla, AcMet or AcGly substrates^{16,17,26,27}. Besides substrate specificities, their subcellular localization appears to be conserved among eukaryotes, as human (HsACPH) and Arabidopsis (AtAARE) AAREs are reported as cytosolic enzymes^{20,21}.

In humans, AARE malfunction is linked to different types of cancer^{26,28,29} and sarcoma cell viability³⁰. Moreover, AARE and proteasomal activity correlate and cooperatively prevent cytotoxic aggregate formation^{31–33}. Several selective inhibitors have been identified^{34,35} and blocking of AARE function is considered as anti-cancer treatment²⁸. Despite an increasing number of studies on AARE functionality in humans, AAREs in plants are far less characterized.

AARE from *Arabidopsis thaliana* (AtAARE) and from cucumber have endo- and exopeptidase functions¹⁷, and silencing of AtAARE increased the levels of oxidized proteins²¹. AtAARE activity was also detected in plastid stroma fractions, although a fusion with a fluorescent reporter did not co-localize with chloroplasts²¹. Suppression of AtAARE *via* RNAi resulted in an enhanced accumulation of oxidized proteins in roots and enhanced electrolyte leakage in leaves, but a further impact on plant physiology was not described²¹.

Moreover, the complete loss of function of this protease has not yet been reported for any organism, neither bacterium,

archaeon, animal, or plant. Thus, although the deep evolutionary conservation of AARE suggests its pivotal role in all major life forms, experimental evidence is far from optimal.

In a proteomics study on protein arginylation we identified an AARE homolog from the moss *Physcomitrella*³⁶. Our further analysis revealed altogether three *Physcomitrella* AARE homologs (PpAARE1–3). Here, we analyzed the subcellular localization of these PpAARE isoforms and of their homolog from the angiosperm *Arabidopsis* (AtAARE). We show that an alternative splicing event is targeting PpAARE1 to chloroplasts, mitochondria, and the cytosol. We provide evidence that an alternative translation initiation is sufficient to localize AtAARE to the same three subcellular compartments. Bioinformatic analyses of several genomes suggest that the localization of AARE in chloroplasts and mitochondria is conserved across the plant lineage. Employing combinatorial gene knockouts and protein co-immunoprecipitation we found distinct interactions between these three isoforms and their concerted action on progressive ageing in *Physcomitrella*. Likewise, an *Arabidopsis* AARE loss-of-function mutant exhibits enhanced levels of oxidized proteins and accelerated bolting, as a hallmark of plant ageing.

Results

AARE gene family expansion and splice variants. Previously, PpAARE1 (Pp1s619_3V6.1) was identified as the most prominent target for N-terminal arginylation in *Physcomitrella*^{36,37}. N-terminal arginylation mediates poly-ubiquitination *via* the N-degron pathway, thus triggering subsequent proteasomal degradation³⁸. Simultaneously, two homologs (PpAARE2: Pp1s108_134V6.1 and PpAARE3: Pp1s97_68V6.1) were identified, although those were not proven arginylation targets³⁶. Meanwhile, a new *Physcomitrella* genome version with chromosome assembly and updated gene versions was released³⁹. Consequently, the gene accessions used here are PpAARE1 (Pp3c2_30720V3.1), PpAARE2 (Pp3c12_21080V3.1), and PpAARE3 (Pp3c7_25140V3.1). According to *OrthoMCL*^{40,41}, all three proteins are homologs of the *Arabidopsis thaliana* acylamino acid-releasing enzyme (AtAARE: AT4G14570). According to publicly available data (<https://peatmoss.online.uni-marburg.de>)⁴² PpAARE1–3 are expressed in all major *Physcomitrella* tissues and developmental stages, although at varying levels (Fig. S1a). Except for leaves (phylloids) and spores, PpAARE1 is the most strongly expressed gene of this family (between 4 and 20 times). In contrast, PpAARE2 is expressed considerably stronger than PpAARE1 and PpAARE3 in spores (Fig. S1a). Likewise, AtAARE is expressed in all major *Arabidopsis* tissues (Fig. S1b, data utilized from Mergner et al.⁴³ and downloaded from <http://athena.proteomics.wzw.tum.de/>). These data indicate a strong, positive correlation between transcript level and protein abundance across all tissues (Fig. S1b). Stress conditions decrease AARE expression in *Arabidopsis* shoots and in *Physcomitrella* protonemata (Fig. S1c–e).

To investigate whether other plants also possess multiple AARE homologs and to infer their phylogenetic relation, we conducted BLASTP⁴⁴ searches against protein models from selected species using the protein sequence of AtAARE as a query. We selected the alga *Chlamydomonas reinhardtii*⁴⁵, the liverwort *Marchantia polymorpha*⁴⁶, the peat moss *Sphagnum fallax* (*Sphagnum fallax* v1.1, DOE-JGI, <http://phytozome.jgi.doe.gov/>), the lycophyte *Selaginella moellendorffii*⁴⁷, the monocot *Oryza sativa*⁴⁸ and the dicot *Populus trichocarpa*⁴⁹, all available at the Phytozome12 database (<https://phytozome.jgi.doe.gov>). Additionally, we performed an NCBI BLASTP search against the charophyte *Klebsormidium nitens* proteome⁵⁰, and identified a single homolog (GAQ80280.1) in this species. We also included proteins of *Funaria hygrometrica*⁵¹, a close relative to *Physcomitrella* from the Funariaceae family⁵², in our search. Finally, the

AtAARE sequence was again searched against the *Physcomitrella*³⁹ and *Arabidopsis*⁵³ proteomes. Homology of the resulting BLAST hits was confirmed if the reciprocal best BLAST hit against *A. thaliana* was again AtAARE.

In *P. trichocarpa*, we identified a single homolog for which three distinct splice variants are annotated (Potri.008G160400.1, Potri.008G160400.2, Potri.008G160400.3). These encode different protein isoforms, but two variants seem to encode non-catalytic proteins. AARE enzymes are prolyl-oligopeptidases with a conserved catalytic triad (Ser/Asp/His) in the C-terminal peptidase domain^{54,55}. In splice variant 2 (Fig. S2, Potri.008G160400.2) alternative splicing results in the deletion of the catalytic Asp whereas the whole catalytic triad is lacking in splice variant 3 (Potri.008G160400.3). Hence, we consider these splice variants as non-active and disregard them from further discussion.

In rice, we identified two homologs (LOC_Os10g28020.3, LOC_Os10g28030.1), with an additional splice variant (LOC_Os10g28020.1) at one locus which encodes an N-terminal extension.

In *C. reinhardtii*, *M. polymorpha*, *S. fallax* and *S. moellendorffii*, we identified a single ortholog each. In *M. polymorpha*, three distinct splice variants are annotated (Mapoly0111s0036.1, Mapoly0111s0036.2, Mapoly0111s0036.3). The latter two are UTR (untranslated region) splice variants, thus resulting in the same protein sequence, whereas Mapoly0111s0036.1 encodes an N-terminal extension of 97 aa compared to the other two variants. In *F. hygroetrica* we identified three distinct isoforms.

Finally, our BLAST searches using the latest *Physcomitrella* protein models³⁹ confirmed three homologs of AtAARE (Pp3c2_30720V3.1, Pp3c12_21080V3.1, Pp3c7_25140V3.1). Additionally, this search revealed another hit, Pp3c1_2590V3.1. This gene is composed of a single exon and encodes a 131 aa protein which harbors the AARE N-terminal domain (PF19283). However, it lacks a catalytic peptidase domain and is hardly expressed across different culture conditions and tissues⁵⁶. We also did not find any proteomics evidence across several *Physcomitrella* analyses^{36,57–59} for this protein. Therefore, we excluded this gene from further analysis.

We then used phylogenetic reconstruction to investigate the origin of gene duplications within the gene family. As an outgroup, we included the well-characterized rat¹⁶ and human²⁶ AARE and two isoforms of the Antarctic icefish *Chionodraco hamatus*²⁷. *Physcomitrella* and *F. hygroetrica* share three distinct pairs of orthologs hinting at an expansion in the common ancestor of the two species. Our phylogenetic analysis did not resolve AARE subfamilies across kingdoms (Fig. 1a) and we conclude that the gene family expansions observed in rice and in the Funariaceae are lineage-specific events.

In addition, this analysis reveals a closer relationship between *PpAARE1* and *PpAARE3*, which presumably originate from a more recent gene duplication event, compared to *PpAARE2*. This is supported by the fact that the open reading frames (ORFs) of *PpAARE1* and *PpAARE3* are represented by a single exon whereas the ORF of *PpAARE2* is split across 17 exons, similar to *AtAARE* (Fig. 1b). This is in congruence with a more recent emergence of intron-poor genes in intron-rich families linked to stress response and developmental processes⁶⁰ and in line with intron-less orphan *Physcomitrella* genes as earliest responders to abiotic stress⁶¹.

For the three *PpAARE* genes, several splice variants are annotated, but only two splice variants of *PpAARE1* give rise to distinct protein isoforms (Fig. 1b; *PpAARE1_1*, *PpAARE1_2*). Both splice variants are present in *Physcomitrella* protonema (Fig. 1b, c), according to RT-PCR with splice variant-specific primers (Supplementary Data S1). Likewise, for *AtAARE* two different ORF definitions exist. With *Araport11*⁶², a new version

of the gene model was introduced exhibiting a longer ORF at the 5' end (Fig. 1b). We detected the full-length transcript via reverse transcription polymerase chain reaction (RT-PCR, Fig. 1c).

For *PpAARE1*, alternative splicing in the 5' end results in an N-terminal truncated variant whereas the longer non-spliced variant encodes an N-terminal plastid transit peptide (cTP) according to *TargetP2.0*⁶³. A cleavage of the transit peptide at the predicted cleavage site (Ala⁷²-M⁷³, Supplementary Data S2) of *PpAARE1* would release exactly the protein encoded by the short splice variant. In contrast, *PpAARE2* and *PpAARE3* do not harbor any predicted N-terminal targeting signals. Moreover, *PpAARE3* is also lacking the WD40 domain that is present in *PpAARE1* and *PpAARE2* (Fig. 1d).

The extension of the originally annotated ORF of *AtAARE* also encodes a plastid transit peptide (Fig. 1d). To our knowledge, the longer variant of *AtAARE* has not yet been investigated, whereas the short variant of *AtAARE* localizes to the nucleus and the cytosol²¹. In agreement with the latter findings, we could predict a nuclear localization sequence (NLS, KKKK) with *LOCALIZER*⁶⁴. Thus, targeting of *AtAARE* to the cytosol and the nucleus, but also to plastids could be enabled by alternative translation initiation. Likewise, *PtAARE* harbors a plastid transit peptide and a potential alternative translation initiation site downstream of the predicted cTP cleavage site.

Accordingly, we checked for NLS in *PpAARE* isoforms and found one (KRRP, Supplementary Data S2) in *PpAARE1* and *PpAARE3*, whereas *PpAARE2* has none, further supporting our hypothesis that *PpAARE1* and *PpAARE3* originate from a relatively recent gene duplication event. Accordingly, alternative splicing also generates two distinct transcripts for *AARE1* in rice (*OsAARE1*, Supplementary Data S2), where one variant encodes a potential plastid transit peptide.

For all other plant species, no plastid targeting sequence was predicted, while the *C. reinhardtii* AARE harbors a mitochondrial targeting sequence (Supplementary Data S2).

PpAARE1 and AtAARE in mitochondria, chloroplasts, and cytoplasm. Organellar targeting of AARE has not yet been reported, although AARE activity was observed in plastid-enriched fractions of cucumber¹⁷. However, chloroplasts, peroxisomes and mitochondria are major hubs of ROS generation⁶⁵, and thus are likely organelles with elevated levels of oxidized proteins. Thus, we investigated whether *PpAARE1* and *AtAARE* would localize to chloroplasts in vivo.

We generated fusion constructs of the *PpAARE* isoforms and of *AtAARE* with eGFP for transient expression in *Physcomitrella* protoplasts. Due to the presence of a predicted plastid targeting peptide for *PpAARE1*, eGFP was fused in frame to the 3' end of all coding sequences (CDS). Since also peroxisomes are ROS-producing organelles, we used *PlantPredPTS1*^{66,67} to check for the presence of C-terminal positioned peroxisomal targeting signals. None of the selected AARE isoforms were predicted to localize to peroxisomes (Supplementary Data S2). Although *AtAARE* has a C-terminal CKL tripeptide, which is experimentally verified to mediate peroxisomal targeting^{66,68}, the properties of its other C-terminal amino acids most likely prevent peroxisomal targeting. A more recent prediction approach for PTS1-mediated targeting for *Arabidopsis* proteins⁶⁹ further supports this conclusion. Peroxisomal targeting can also be mediated via N-terminal nona-peptides^{70,71}, but these motifs are also not present within the first 100 aa in any of the selected AARE sequences. In agreement with these predictions eGFP was fused to the 3' end of the CDSs.

For *PpAARE1* three different fusion constructs were assembled. Among these, a fusion of the CDS of the short splice

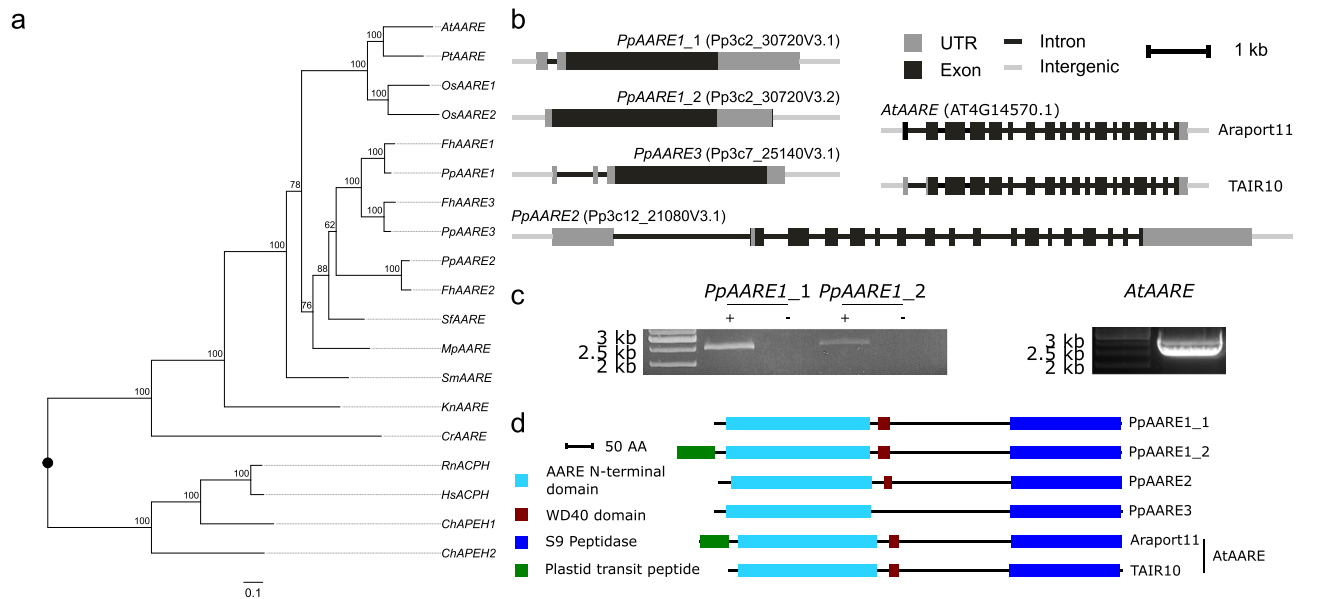


Fig. 1 Phylogenetic tree for AARE isoforms from selected organisms, gene structures, and proteins domains of *P. patens* and *A. thaliana* AARE isoforms. **a** Maximum likelihood tree based on an alignment of multiple AARE coding sequences. Duplication events in several species appear to be lineage-specific. Node values reflect percentage confidence values based on 1000 bootstrap replicates. Species abbreviations: At: *Arabidopsis thaliana*; Pt: *Populus trichocarpa*; Os: *Oryza sativa*; Pp: *Physcomitrium patens*; Fh: *Funaria hygrometrica*; Sf: *Sphagnum fallax*; Mp: *Marchantia polymorpha*; Sm: *Selaginella moellendorffii*; Kn: *Klebsormidium nitens*; Cr: *Chlamydomonas reinhardtii*; Rn: *Rattus norvegicus*; Hs: *Homo sapiens*; Ch: *Chionodraco hamatus*. **b** Gene structure of PpAARE1-3 and AtAARE. For PpAARE1 two splice variants exist. For AtAARE two different 5' UTR definitions are present (upper: Araport11⁶²; lower: TAIR10⁵³). **c** Left: Both splice variants of PpAARE1 were amplified from complementary DNA (cDNA); +: with cDNA template; -: without reverse transcriptase. Expected amplicon size: PpAARE1_1: 2512 bp; PpAARE1_2: 2596 bp. Primers were designed to be specific for the splice variants (Supplementary Data S1). Right: the longer open reading frame of AtAARE was amplified from cDNA. Expected amplicon size: 2457 bp (Supplementary Data S3). **d** Protein structures showing PFAM-domains for PpAARE1-3 and AtAARE. All isoforms contain an AARE N-terminal domain (PF19283) and a catalytic Peptidase S9 domain (PF00326). PpAARE1, PpAARE2, and AtAARE additionally contain a WD40 domain (PF07676). The long splice variant of PpAARE1 and the longer open reading frame of AtAARE encode a predicted N-terminal plastid transit peptide (cTP). AA amino acid. Cleavable N-terminal sequences were predicted by TargetP2.0⁶³.

variant (Pp3c2_30720V3.1) and eGFP was cloned, as well as a fusion of the CDS of the longer splice variant (Pp3c2_30720V3.2) and eGFP. Additionally, we cloned a fusion of eGFP and the sequence part in which both variants differ (M¹-A⁷², Pp3c2_30720V3.2). This part harbors the plastid transit peptide predicted by TargetP2.0. All fusion constructs were expressed under the control of the Physcomitrella Actin5 promoter^{57,72} in a pMAV4 plasmid backbone⁷³.

The PpAARE1 isoform derived from the short splicing variant (PpAARE1_1, Fig. 1b) clearly localized to the cytoplasm (Fig. 2). The same localization was observed for PpAARE2 and PpAARE3 (Fig. 2). Despite a predicted NLS, we did not observe a nuclear localization, either for PpAARE1 or for PpAARE3.

The isoform encoded by the longer splice variant of PpAARE1 (PpAARE1_2, Fig. 1b) localized to chloroplasts and surprisingly also to mitochondria (Fig. 2). In contrast to the diffuse cytosolic distribution of PpAARE1, specific foci were observed in chloroplasts. To investigate whether the N-terminal sequence differing between the two PpAARE1 variants (M¹-A⁷², Pp3c2_30720V3.2) is sufficient to confer dual targeting, we fused this N-terminal sequence 5' to eGFP and observed again dual localization (Fig. 2, PpAARE1_Nt). Full-length PpAARE1 was necessary to localize eGFP to foci within chloroplasts, as the PpAARE1_Nt:eGFP fusion led to a uniform distribution. However, full-length PpAARE1 was also homogeneously distributed throughout the cytoplasm. This indicates the presence of interactors that recruit PpAARE1 to specific sites or complexes within the chloroplasts. Further, we conclude that the N-terminal extension of PpAARE1_2 encodes an ambiguous targeting signal for import into chloroplasts and mitochondria as it is capable of

directing the fusion protein simultaneously to both organelles. Based on this data, PpAARE1 is targeted to three organelles: chloroplasts, mitochondria and the cytosol. To independently scrutinize these findings, we measured AARE enzyme activity in the organelles. Using organelle fractionation as previously described⁷⁴, we detected AARE activity in chloroplasts, the cytosol, and mitochondria, although to a lesser extent in the latter (Fig. S3). Thus, in vivo localization of fusion proteins and enzyme measurements after cell fractionation independently confirm the predicted triple localization of AARE in Physcomitrella.

Simultaneous localization of proteins to chloroplasts and mitochondria can be mediated via ambiguous targeting signals which are recognized by both translocation machineries. We evaluated whether ATP2⁷⁵, a tool for the prediction of ambiguous targeting, would recognize PpAARE1 but this was not predicted to be dually targeted. In contrast, AtAARE was predicted to be dually targeted via an ambiguous signal. Thus, we cloned the analogous three fusion constructs for AtAARE and investigated the subcellular localization of their encoded proteins accordingly.

The AtAARE isoform translated from the shorter ORF (AtAARE, Fig. 1b) localized to the cytoplasm (AtAARE_SV, Fig. 2), as observed for PpAARE1_1. This result is partially in agreement with Nakai et al.²¹ since we could not observe nuclear localization. Using the fusion construct of the longer AtAARE variant, we observed clear dual targeting of the protein to chloroplasts and mitochondria (AtAARE_LV, Fig. 2), as observed for PpAARE1_2. Here, the eGFP signal was distributed homogeneously in the chloroplasts, in contrast to the foci of PpAARE1:eGFP.

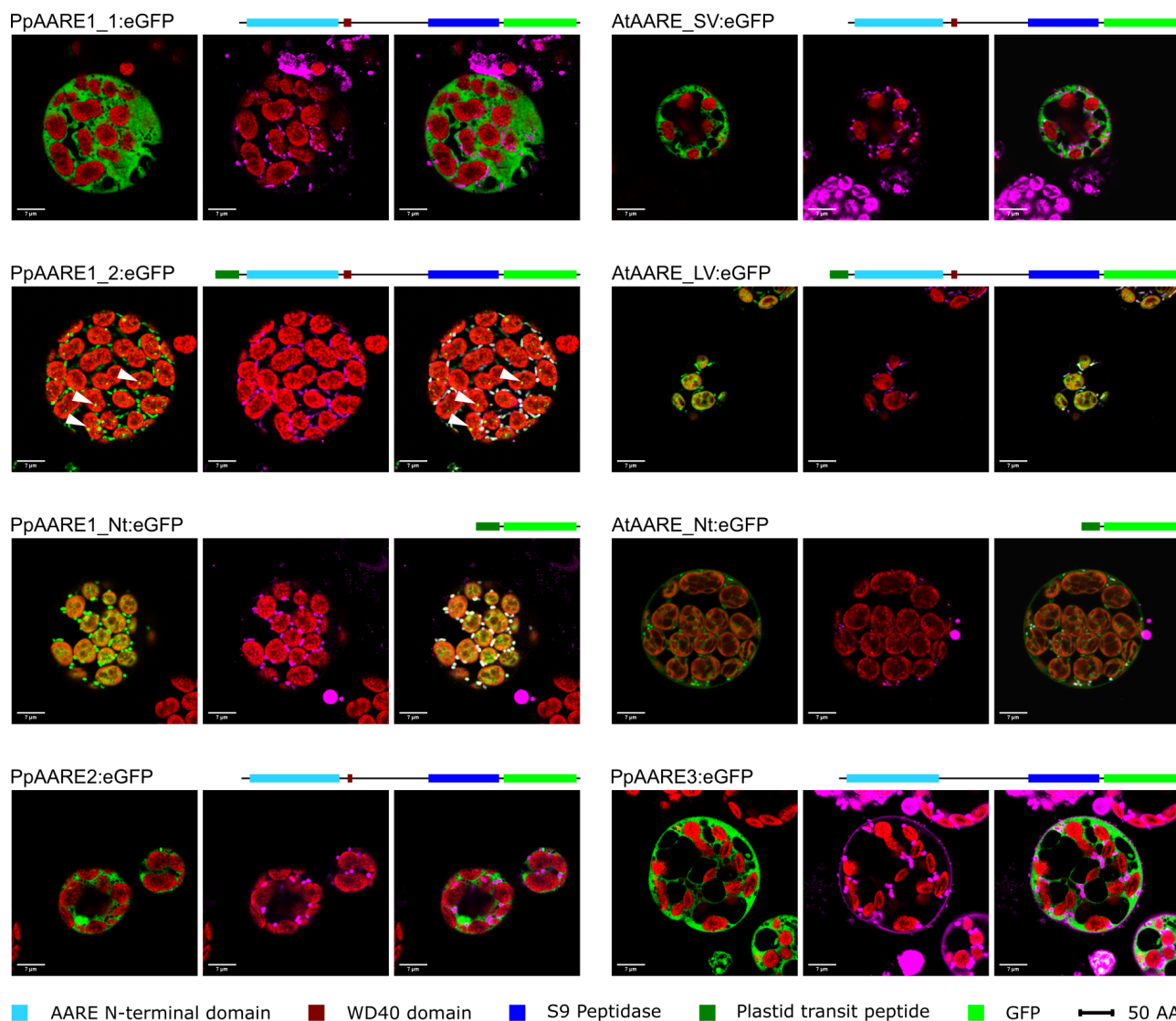


Fig. 2 Confocal microscopy images showing the localization of PpAARE isoforms and AtAARE with C-terminal fused eGFP in *Physcomitrella* protoplasts. Fusion proteins with domain structures are depicted. PpAARE1_1, PpAARE2, and PpAARE3 localize to the cytoplasm. PpAARE1_2 localizes to specific foci in plastids (white arrows) and to mitochondria. The N-terminal extension of PpAARE1_2 encoding a predicted plastid transit peptide (PpAARE1_Nt) directs eGFP to plastids and mitochondria. The short variant of AtAARE (SV) localizes to the cytoplasm. The long variant (LV) localizes to plastids and mitochondria. The N-terminal extension of the long variant of AtAARE localizes to plastids and mitochondria. Left image: chlorophyll autofluorescence (red) and eGFP (green). Middle image: chlorophyll autofluorescence (red) and MitoTracker™ (magenta). Right image: chlorophyll autofluorescence (red), eGFP (green), MitoTracker™ (magenta) and co-localization of eGFP and MitoTracker™ (white). Bars = 7 μm.

Next, we cloned only the N-terminal sequence differing between both variants (M^1 -A⁵⁵, longer ORF definition, Fig. 1b) and fused it to eGFP. In order to investigate whether the exact N-terminal difference between the two AtAARE variants would be sufficient for targeting, the M⁵⁶ (same as M¹ in the shorter variant), which is the PI aa at the predicted cleavage site, was deleted. Using this construct, the eGFP signal localized to chloroplasts and mitochondria (AtAARE_Nt, Fig. 2). The signal within chloroplasts was homogeneously distributed, similar to the longer AtAARE variant. Thus, we conclude that the N-terminal extension of both long PpAARE and AtAARE variants is sufficient for dual targeting of proteins *in vivo*. Intriguingly, the longer variant of AtAARE localized exclusively to chloroplasts and mitochondria although alternative translation initiation should be possible. This is interesting as alternative translation initiation is also possible in the longer splice variant of PpAARE1 (PpAARE1_2). In the latter also, the fusion protein localizes

exclusively to chloroplasts and mitochondria, which excludes the possibility of an alternative translation initiation, at least in protoplasts. There are numerous transcripts in mammals where translation of an upstream positioned ORF suppresses the translation of the downstream main ORF⁷⁶. A similar scenario is conceivable in *Physcomitrella*. However, it remains unclear how and if translation from the internal start codons is controlled. It is also possible that factors controlling alternative translation initiation of AtAARE are absent in *Physcomitrella*, at least in a spatiotemporal manner, or they might only be triggered in specific physiological situations. According to our data, the translation of the two variants of PpAARE1 is mainly controlled by alternative splicing and not by alternative translation initiation.

In summary, PpAARE1 and AtAARE localize to three subcellular compartments via an ambiguous targeting signal. In contrast, PpAARE2 and PpAARE3 localize solely to the cytoplasm.

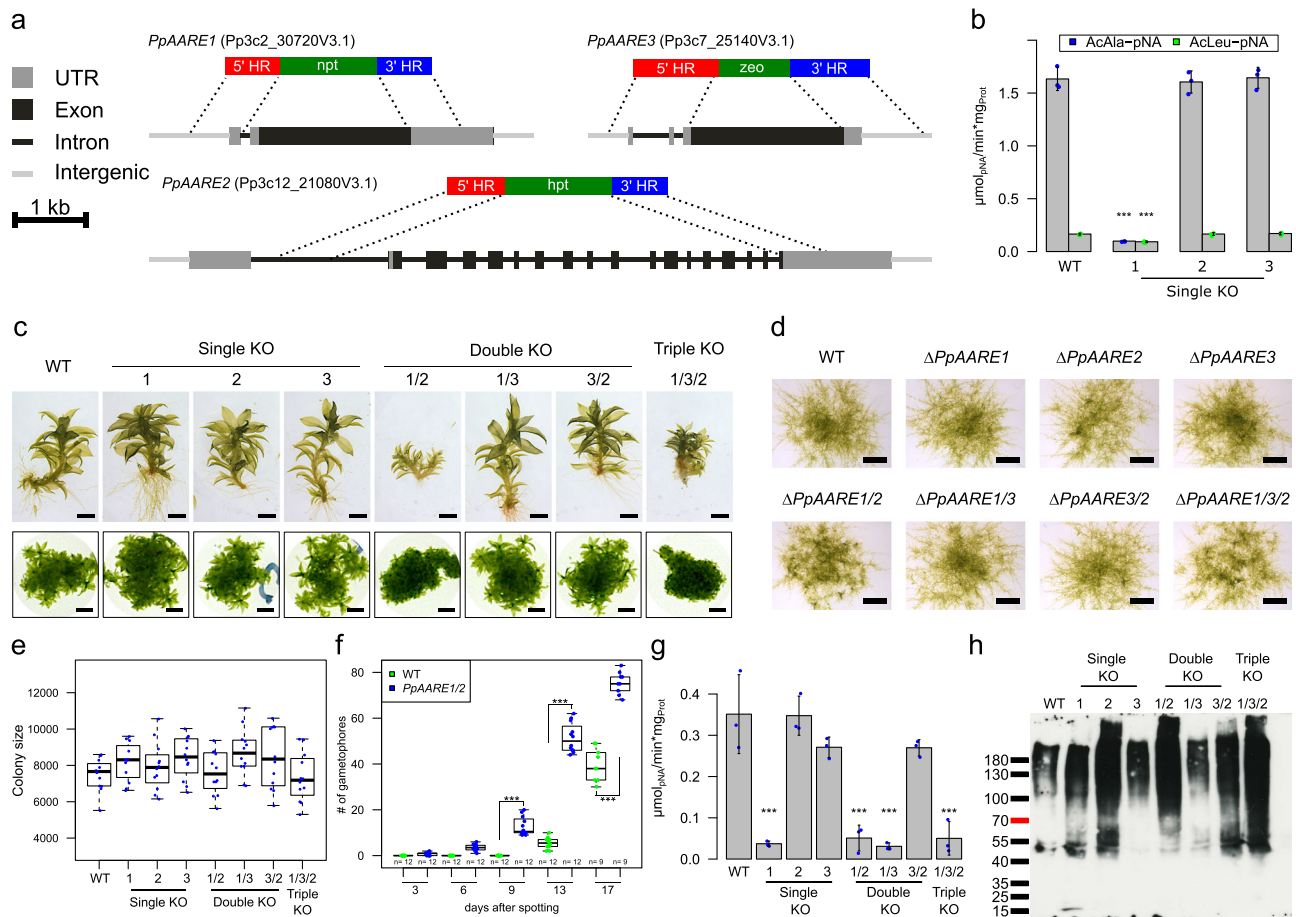


Fig. 3 Phenotype analyses, AARE activity and level of oxidized proteins in *Physcomitrella* WT and KO mutants. **a** Each isoform was knocked out using a different selection marker. The selection markers confer resistance against G418 (npt), hygromycin (hpt) and zeocin (zeo), respectively. Homologous regions (HR) were chosen in order to remove the full CDS of the corresponding gene upon integration of the selection marker. **b** Mean AARE activity on AcAla-pNA in *Physcomitrella* protonema with standard deviation ($n =$ three biological replicates). Significance levels are based on a one-way Anova and subsequent post-hoc test ($***p < 0.001$) and indicate differences compared to WT. **c** Phenotypes of gametophores of WT and the different KOs cultivated on KnopME for 4 months. All colonies were grown on the same plate. Upper panel: Bar = 0.5 mm; lower panel: Bar = 2 mm. **d** Protonema colonies grown on KnopME with 0.02% glucose taken from suspension culture. Bar = 1 mm. Images were taken 9 days after spotting. **e** Box plot showing the distribution of colony areas ($n = 12$ colonies per box plot; colony images taken 7 days after spotting). No significant difference of colony areas between WT and the KOs was observed (tested via one-way Anova). **f** Box plot showing the number of gametophores per colony and day of WT and $\Delta PpAARE1/2$. Counting was performed at indicated days after spotting protonema suspension culture on solid medium (KnopME with 0.02% glucose). Indicated significance levels are based on a two-way Anova with subsequent post-hoc test ($***p < 0.001$). The box plots (**e**, **f**) depict the mean (horizontal bold line) of the data, the interquartile range (box) and the 1.5x interquartile range (whiskers). **g** Mean AARE exopeptidase activity on AcAla-pNA in gametophores. Depicted is the mean of three independent colonies per line with standard deviations. All colonies were cultivated on the same plate (Fig. S7a). Significance levels are based on one-way Anova and indicate differences compared to WT ($***p < 0.001$). **h** Levels of oxidized proteins in gametophores of WT and the different KOs (Coomassie-stained loading control is shown in Fig. S7b). The analysis was repeated three times (additional blots available in Fig. S7c, d). Detection of oxidized proteins was performed with the OxyBlot™ Protein Oxidation Detection Kit (Merck).

Double knockout of *PpAARE1/2* reduces lifespan. Null mutants of AARE have not been described in any organism, and the biological role of this protease apart from its catalytic function remained unclear. Hence, we created AARE knockouts in *Physcomitrella* by deleting the full CDS of each gene *via* gene targeting (Fig. 3a) according to⁷⁷. To enable subsequent knockout (KO) of other AARE genes, different selection markers were used. Since three distinct AARE genes exist in *Physcomitrella* which result in cytosolic proteases, we generated all possible combinations of double KOs and triple KOs to avoid potential compensation of the loss of function.

Plants surviving the selection procedure were screened via PCR for the absence of the respective CDS and correct integration of the KO construct in the target locus (Fig. S4a). Additionally, the number of genomic integrations of the KO construct was

measured *via* quantitative PCR (qPCR) as described⁷⁸ (Fig. S4b). At least three independent lines were identified for all single, double and triple KOs (Fig. S4c–i) and a line with only a single integration in the genome was detected for each KO (j–p, line numbers with stars). Further, haploidy of all lines was confirmed *via* flow cytometry (Fig. S5a–c) as described⁷⁹. These precautions were made as the transformation procedure may generate plants with multiple integrations⁸⁰, possibly leading to off-target effects. Further, the transformation procedure may lead to diploid plants with altered gene expression⁸¹. We used haploid lines with a single integration of the KO construct (Fig. S4) for subsequent experiments.

Typically, AARE exopeptidase activity is assayed *via* N^α-acetylated amino acids like AcAla or AcMet coupled to a reporter such as para-nitro-anilide (pNA) or 7-amido-4-methylcoumarin

(AMC). From these, AcAla-pNA was tested for several eukaryotic AAREs^{22,26}, including AtAARE¹⁷. Here, we analyzed the impact of AARE loss of function on the activity towards AcAla-pNA and AcLeu-pNA. The latter is a substrate of bacterial and archaeal AARE isoforms but also eukaryotic isoforms exhibit cleavage activity on this substrate^{16,22–25}. On the single KO level, the exopeptidase activity on both substrates was significantly reduced in the $\Delta PpAARE1$ mutant whereas the single KO of the other isoforms did not affect the activity (Fig. 3b). This strong impact of PpAARE1 on the exopeptidase activity was consistent across all transgenic mutant lines (Fig. S6).

One important step in *Physcomitrella* development is the transition from protonema to gametophores, a developmental progression regulated among others by plant age and the nutrient status⁸². The single KOs were phenotypically inconspicuous on the gametophore level (Fig. 3c). In contrast, gametophores of $\Delta PpAARE1/2$ and $\Delta PpAARE1/3/2$ were severely stunted and colonies were denser compared to wild type (WT) or the other mutants (Fig. 3c). This growth effect is restricted to gametophores since protonema growth on solid medium did not differ between WT and the KOs (Fig. 3d, e). Intriguingly, $\Delta PpAARE1/2$ and $\Delta PpAARE1/3/2$ mutants showed accelerated developmental transition, as they developed gametophores from protonema earlier (Fig. 3d). Since other KO lines did not show this effect, we attributed this to the double KO of *PpAARE1/2* and performed a quantitative comparison with WT. Here, gametophores were already observed after 6 days in the double KO of *PpAARE1/2*, while in WT a similar number of gametophores per colony was observed only after 13 days (Fig. 3f). Consequently, the double KO of *PpAARE1/2* causes accelerated developmental progression but gametophores remained ultimately smaller than in WT (Fig. 3c). These effects are not linked to AARE exopeptidase activity since the exopeptidase activity in gametophores was significantly reduced in all lines with a KO of PpAARE1 (Fig. 3g), which mimics the activity profile in protonema (Fig. S6).

To analyze AARE endopeptidase activity, we assessed the total levels of oxidized proteins in gametophores. In this assay, protein carbonyl groups derived from oxidation are derivatized with 2,4-dinitrophenylhydrazine (DNPH) to 2,4-dinitrophenylhydrazone (DNP). This irreversible modification is then recognized on Western blots by a primary anti-DNP antibody. Since DNPH can also react with oxidation states of cysteine side chains⁸³, this assay detects not only protein carbonylation but general protein oxidation.

With this assay we found that PpAARE2 had the strongest impact on the level of oxidized proteins in gametophores (Fig. 3h) and thus is not linked to exopeptidase activity. This was consistently observed in three independent analyses (Fig. 3h, Fig. S7). Apparently, PpAARE3 does not have any impact on exopeptidase and endopeptidase activity in gametophores under standard conditions (Fig. 3g, h).

Taken together, PpAARE1 predominantly acts as exopeptidase, while PpAARE2 predominantly acts as endopeptidase, and only the simultaneous loss of both activities in the double knockout mutants has the severest phenotypical consequences.

We found another remarkable difference between WT and mutants with a double KO of *PpAARE1/2* in older plants. After 5 months of cultivation, $\Delta PpAARE1/2$ and $\Delta PpAARE1/3/2$ were only viable at the tip of the gametophores (Fig. 4a), whilst most of the colony was already dead. In contrast, gametophores of WT and the other KOs were fully viable. After 8 months, $\Delta PpAARE1/2$ and $\Delta PpAARE1/3/2$ were already dead, in contrast to WT and the respective parental lines, which only showed some dead gametophores (Fig. 4b, c).

In summary, mutants with a double KO of *PpAARE1/2* exhibit accelerated developmental transition from protonema to

gametophore (Fig. 3f), while size and life span of gametophores is strikingly reduced (Figs. 3c and 4a–c). In contrast, these effects are not visible in $\Delta PpAARE1/3$. Therefore, these ageing phenotypes are linked to the concurrent loss of major AARE endopeptidase and exopeptidase activity.

Distinct in vivo interactions of PpAARE isoforms. In different organisms, AARE forms different homomeric complexes such as dimers¹⁴, tetramers¹⁷, or hexamers²⁴. Thus, we analyzed whether the PpAARE isoforms can interact with each other. Previously, all three isoforms were identified, although the protein modification used for pulldown (N-terminal arginylation) was only identified on PpAARE1³⁶. This gave rise to two hypotheses: First, PpAARE2 and PpAARE3 are also targets for N-terminal arginylation, but modified peptides were not identified for these isoforms. Second, the isoforms interact in complexes which were pulled down due to the N-terminal arginylation of PpAARE1. We generated Citrine fusion lines for each isoform via in-frame tagging at the native locus (knock-in, Fig. 5a). The original stop codons of the respective PpAARE CDS were deleted. The Citrine-tag was intended for two different analyses: First, it should enable in vivo monitoring of PpAARE isoforms expressed from the native promoter, and second, it is a valid tag for co-immunoprecipitation (Co-IP) via commercially available trap-beads.

In plants with a detectable fusion transcript (Fig. S8a–c) the presence of the target protein was checked via IP and subsequent MS analysis. For *PpAARE3:Citrine* lines, we detected transcripts in one line and obtained only insufficient coverage and intensity at the MS across several Co-IPs. Thus, these *Physcomitrella* lines were excluded from further analysis. The co-precipitation of other PpAARE isoforms with the respective bait isoforms was observed in test IPs (Fig. S8d, e) confirming previous MS-Data³⁶. All plants harboring the Citrine fusion were phenotypically inconspicuous (Fig. S8f) and haploid (Fig. S8g). Although the fusion proteins were detected in two independent lines for each of the two isoforms (PpAARE1, PpAARE2), we could not observe any Citrine signal within *Physcomitrella* protonemata or gametophores, probably due to the low abundance of the PpAARE isoforms. Nevertheless, MS intensities and sequence coverage enabled quantitative Co-IPs. The MS data have been deposited in PRIDE^{84,85} with the accession codes PXD033854 and PXD038742.

When targeting PpAARE1:Citrine, both other isoforms appeared as significant interacting partners (Fig. 5b, $p < 0.01$, FDR = 0.01). In a reciprocal Co-IP targeting PpAARE2:Citrine only, PpAARE1 appeared as significant interacting partner. PpAARE3 was not detected in this pulldown. Although lacking a reciprocal IP targeting PpAARE3:Citrine, the data show that PpAARE1 interacts with PpAARE2 and PpAARE3, whereas PpAARE2 only interacts with PpAARE1. Consequently, there are distinct interactions of PpAARE1 with PpAARE2 and PpAARE3 in vivo, possibly resulting in cytosolic heteromeric AARE complexes in *Physcomitrella*.

AARE affects bolting time in Arabidopsis. In *Physcomitrella* three AARE genes exist, and the concerted action and interaction of the enzymes affect plant ageing. To evaluate if this is an evolutionary conserved function, we analyzed the situation in *Arabidopsis*. Here, it was known that silencing of the single AARE gene leads to an accumulation of oxidized proteins, whereas overexpression did not affect their levels²¹. To gain deeper insights, we screened for available *Arabidopsis* T-DNA mutants.

We identified two T-DNA insertion lines (SALK_071125 and GK-456A10) in the T-DNA Express database at the SIGnAL website (<http://signal.salk.edu>). SALK_071125 (s68) has a T-DNA

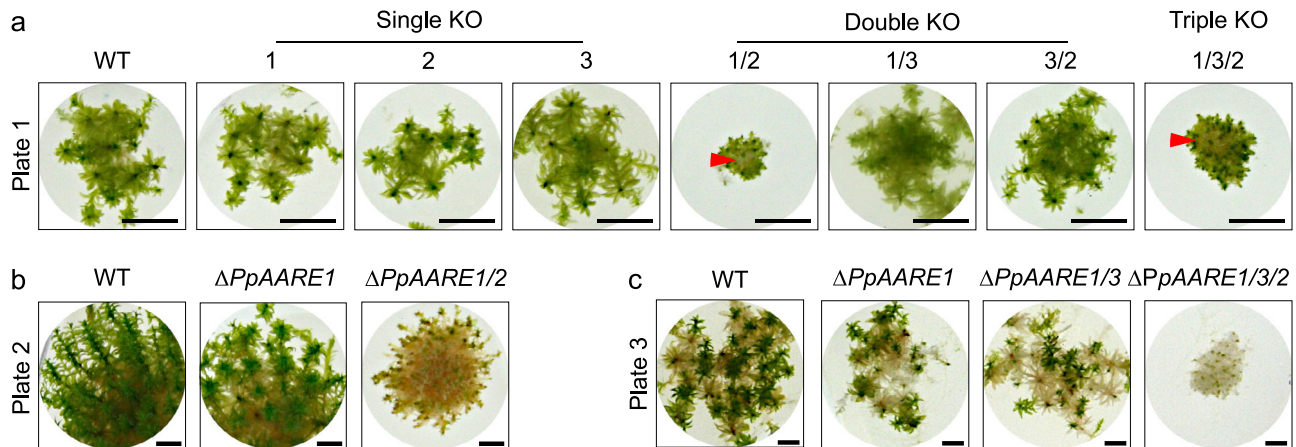


Fig. 4 Physcomitrella gametophore colonies of varying age. **a** Colonies of all representative knockout mutants after 5 months on solid medium (KnopME). Bar = 5 mm. Gametophores of $\Delta PpAARE1/2$ and $\Delta PpAARE1/3/2$ are only viable at the tip, whereas plant material at the base (red arrow) is dead. **b** Colonies after 8 months on solid medium. $\Delta PpAARE1$ is the parental line for $\Delta PpAARE1/2$. Gametophores of WT and $\Delta PpAARE1$ are still viable whereas $\Delta PpAARE1/2$ gametophores are mostly dead. Bar = 2 mm. **c** Colonies after 8 months on solid medium. $\Delta PpAARE1$ is the parental line for $\Delta PpAARE1/3$ and $\Delta PpAARE1/3$ is the parental line for $\Delta PpAARE1/3/2$. Colonies of WT, $\Delta PpAARE1$ and $\Delta PpAARE1/3$ still have viable gametophores, whereas $\Delta PpAARE1/3/2$ gametophores are dead. Bar = 2 mm.

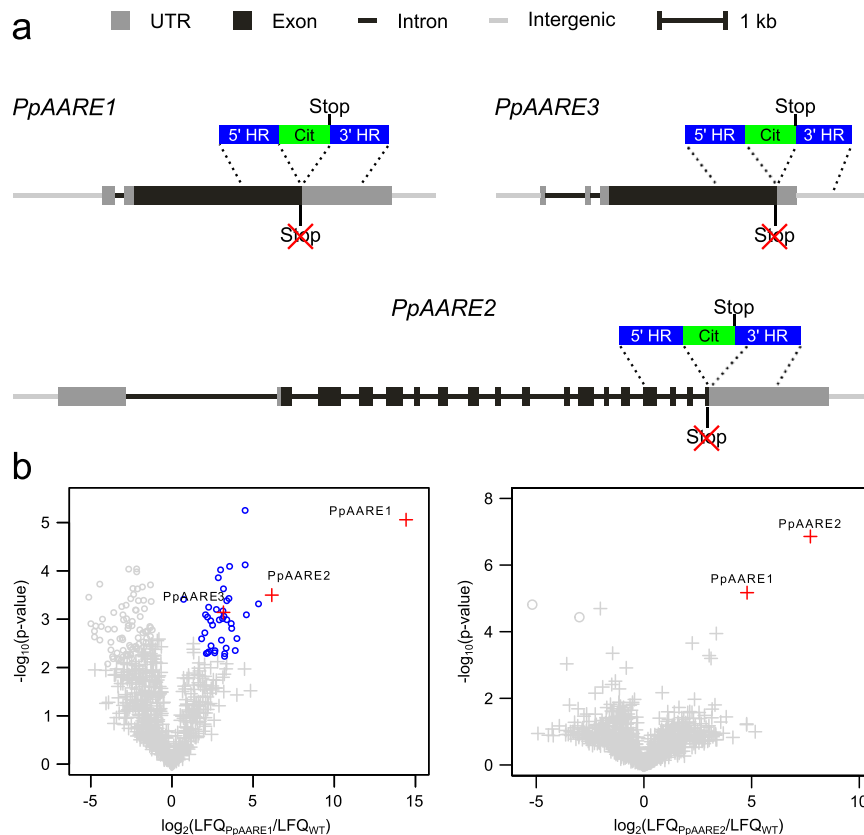


Fig. 5 Reciprocal co-immunoprecipitation (Co-IP) with Citrine-tagged PpAARE isoforms. **a** Tagging of PpAARE isoforms was realized by in-frame fusion with a linker-Citrine CDS at the respective native locus *via* homologous recombination. Original stop codons were deleted. **b** Volcano plots showing the result of the Co-IPs against each of the PpAARE:Citrine fusion proteins. Left panel: Pulldown of PpAARE1:Citrine. Right panel: pulldown of PpAARE2:Citrine. Co-IP was performed with GFP-Trap Magnetic Particles M-270 (Chromotek) and protonema from suspension culture. Log₂ ratios of normalized label-free quantitation values (LFQ) are plotted against $-\log_{10}$ of adjusted *p*-values. Proteins significantly enriched in the Citrine-tagged pulldown are shown in blue circles ($p < 0.01$, FDR = 0.01). Significantly enriched PpAARE isoforms are depicted as red crosses.

insertion in an intron at the 5' UTR, whereas the T-DNA insertion in GK-456A10 (GK) maps to an intron in the region encoding the catalytic domain (Fig. 6a). We obtained these mutants, identified homozygous populations of GK-456A10

containing the T-DNA insertion by their resistance to sulfadiazine, and confirmed their genotype by PCR. In the case of the Salk line (s68), homozygous plants had lost their resistance to kanamycin, but we confirmed their genotype by PCR.

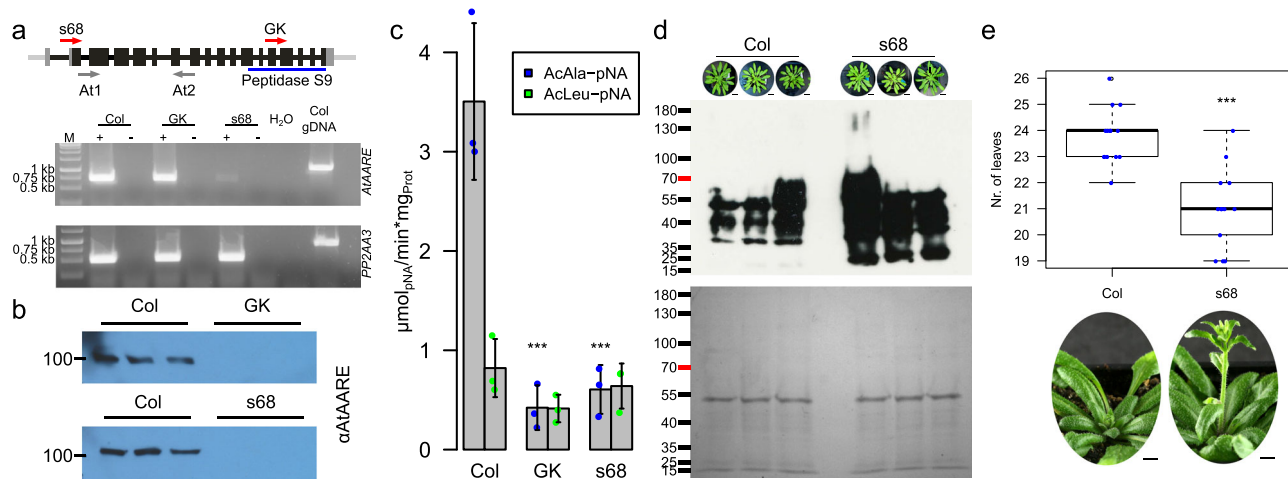


Fig. 6 Molecular and phenotypical characterization of *A. thaliana* T-DNA mutant lines. **a** Structure of the AtAARE gene and positions of T-DNA insertions (red arrows indicate positions of T-DNA insertion, s68 (SALK_071125) and GK (GK-456A10)) and primers (At1, At2) used for RT-PCR (below). Transcription analysis of AtAARE was performed by RT-PCR in WT (Col), s68, and GK plants. Negative controls without reverse transcriptase (-), a water control (H₂O) and genomic DNA control (gDNA) are indicated. Expected amplicon sizes: AtAARE: cDNA 739 bp, gDNA: 1204 bp; PP2AA3 (reference gene): cDNA: 517 bp, gDNA: 911 bp. Primers are listed in Supplementary Data S3. **b** Western blot analysis on extracts of the two T-DNA mutants and WT probed with a polyclonal anti-AARE antibody. In both T-DNA lines AtAARE is not detectable. Full blot images are available in Fig. S10. **c** Mean exopeptidase activity in *A. thaliana* extracts on AcAla-pNA and AcLeu-pNA with standard deviation ($n = 3$ biological replicates). Significance levels are based on one-way Anova and subsequent post-hoc test ($***p < 0.001$) and indicate differences compared to WT (Col). **d** Detection of oxidized proteins in WT (Col) and AtAARE mutant (s68). From three independent plants one exterior rosette leaf was taken after cultivation for 8 weeks in short-day conditions (8 h light/16 h dark). Bars correspond to 2 cm. Protein loading control by Coomassie staining is depicted below. **e** Box plot of the bolting analysis of WT (Col, $n = 14$) and AtAARE mutant plants (s68, $n = 13$). The box plot (**e**, **f**) depicts the mean (horizontal bold line) of the data, the interquartile range (box) and the 1.5x interquartile range (whiskers). Outliers are depicted as white dots. Significance level is based on a one-way Anova and subsequent post-hoc test ($***p < 0.001$). Exemplary plants (45-day-old plants grown in long-day conditions, 16 h light/8 h dark) are depicted below the box plot. Bars correspond to 1 cm.

Homozygous plants of both genotypes were back-crossed with WT Col-0, and brought to homozygosity for subsequent experiments. Primers for screening and validation of both T-DNA lines are listed in Supplementary Data S3. Additionally, we analyzed AARE gene expression *via* RT-PCR. The transcript was still detectable in both lines (Fig. 6a), although very reduced in s68, while the protein was not detectable via Western blot (Fig. 6b). Surprisingly, in WT AARE was detected at around 100 kDa, although the estimated molecular weight is ~84 kDa (90 kDa for the longer ORF variant without cleavage of the plastid targeting peptide) which indicates the presence of posttranslational modifications. Phenotypically, neither seedlings nor adult mutant plants showed obvious deviations from WT (Col, Fig. S9).

Next, we assayed AARE exopeptidase function in Arabidopsis WT and the two mutants. The exopeptidase activity on AcAla-pNA was significantly reduced in both T-DNA mutants. In contrast, the activity on AcLeu-pNA did not change significantly, although a slight reduction was observed in the GK line (Fig. 6c). Thus, in agreement with Western blot and activity data, the remaining transcripts detected *via* RT-PCR (Fig. 6a) are not translated to functional enzymes, suggesting complete loss of AARE function in the mutants. Based on this characterization, we concentrated on T-DNA mutant s68.

Subsequently, we assayed the AARE endopeptidase activity in Arabidopsis. The most striking feature reported were increased levels of oxidized proteins in AARE-silenced Arabidopsis plants²¹ which is in line with our findings in *Physcomitrella* AARE mutants. To corroborate this, we investigated levels of oxidized proteins in the Arabidopsis T-DNA mutant (s68) in comparison to WT (Col) cultivated under short day conditions. In both genotypes, the distribution of oxidized proteins was different to *Physcomitrella* gametophores (Fig. 6d). Using the same extraction protocol, oxidized proteins in Arabidopsis were mainly of lower

molecular weight, whereas in *Physcomitrella* they were mainly at higher molecular weight (Fig. 3h). Despite these size differences, the level of oxidized proteins was higher in the Arabidopsis mutant than in WT (Fig. 6d), mimicking the situation in *Physcomitrella*. Together, we found AtAARE exopeptidase and endopeptidase activity to be reduced in our experiments.

Oxidized proteins accumulate during vegetative growth of Arabidopsis and are depleted at the transition to bolting⁸⁶. It was not clear from this study whether the level of oxidized proteins is a signal for bolting, or if the reset of protein oxidation at the bolting transition is a side-effect of enhanced protein turnover during this process. To address this, we assessed the bolting behavior of Arabidopsis WT and mutant plants and found that bolting in mutant plants differed significantly from WT. In WT, bolting started at 24 ± 1 rosette leaves whereas it started at 21 ± 2 rosette leaves in the mutants (Fig. 6e). Consequently, this accelerated developmental transition in the mutants correlates with enhanced levels of oxidized proteins.

Discussion

A universal definition of ageing is difficult due to strongly differing characteristics between and within the domains of life. In humans, the term ageing is inherently linked to degenerative diseases whereas plant ageing is considered as the progression of developmental transitions from seeds to senescence. Nevertheless, a common feature of ageing is the execution of a genetic program that controls growth, development and maturation. In turn, the progression of this genetic program depends on the metabolic state and environmental factors. Among the molecules responsible for ageing are ROS. Their involvement in ageing and diseases was first postulated by Harman⁸⁷ and was extended by considering mitochondria as central sources⁸⁸. In humans,

mitochondrial malfunction in line with increased ROS levels is a central determinant of ageing and associated pathologies⁸⁹. In plants, mitochondrial ROS increase during ageing of seeds⁹⁰ and are major determinants of germination capacity⁹¹. In photosynthetic tissues chloroplasts are the major source of ROS and their levels increase during ageing^{92–94}. Plants cannot escape from stress situations that increase ROS production to detrimental levels, and despite several layers of ROS defense, oxidized proteins constitute the major share of modified molecules under stress. Consequently, protein oxidation and subsequent aggregate deposition are hallmarks of ageing^{95,96}. The degradation of artificially oxidized proteins by AARE has been demonstrated repeatedly, and silencing of *AtAARE* in turn increased the levels of oxidized proteins^{19–22}.

However, the contribution of AARE to the progress of ageing remained elusive, although several studies associate AARE function to age-related diseases^{97–99}. Here, we identified three *AARE* genes in *Physcomitrella*. This gene family expansion is an outstanding feature of the moss family Funariaceae, as most organisms we analyzed contain only a single *AARE* gene, and only a few have two. We analyzed these three isoforms in *Physcomitrella* and compared selected features to the single isoform in *Arabidopsis*. Our data reveal specific functions in age-related developmental transitions and life span determination.

Surprisingly, we found triple localization of *AtAARE* and *PpAARE1* to chloroplasts, mitochondria and the cytosol *in vivo*, suggesting a functional role for AARE in these cellular compartments. In *Physcomitrella*, the triple localization is mediated via alternative splice variants and in *Arabidopsis* likely via alternative translation initiation. Although there have been indications of *AtAARE* being associated to chloroplasts^{17,21}, there was no clear evidence for organellar targeting of this protease until now. It is remarkable that the triple localization of AARE is evolutionary conserved between *Arabidopsis* and *Physcomitrella*, although likely executed via different molecular mechanisms. This suggests an essential and evolutionary conserved function of AARE activity in the cytoplasm, chloroplasts and mitochondria. As mosses and seed plants diverged more than 500 million years ago¹⁰⁰, this is a deep evolutionary conservation.

Previously, AARE exopeptidase activity was observed in cucumber chloroplasts¹⁷, and AARE peptides were found in proteomes of *Arabidopsis* chloroplasts¹⁰¹ and mitochondria¹⁰². In contrast, AARE was not identified in plastid or mitochondrial proteomes of *Physcomitrella*^{57,59}. We found AARE exopeptidase activity in chloroplasts and mitochondria of *Physcomitrella*. Chloroplasts are a major source of ROS in photosynthetic tissues exposed to light, whereas mitochondria are the major source of ROS in non-photosynthetic tissues or in the dark^{93,94,103,104}. Until now, it remained unresolved how plants deplete oxidized proteins from these organelles.

In yeast and mammals, the ATP-dependent LON and AAA proteases are involved in clearance of misfolded and oxidized mitochondrial proteins. Intriguingly, mutants of plant homologs of LON proteases did not show clear effects on the levels of oxidized proteins, but AAA-type FTSH proteases may play a role¹⁰⁵. Nevertheless, stressors such as heat, drought or intense light compromise photosynthesis^{106,107} and mitochondrial respiration¹⁰⁸, leading to a depletion of ATP and to mitochondrial dysfunction¹⁰⁹. In turn, energy supply for ATP-dependent defense systems such as heat-shock proteins and AAA-type proteases is severely compromised, leaving the question unanswered how oxidized proteins in chloroplasts and mitochondria can be cleared. Because AARE is an ATP-independent protease, our data suggest that organellar-targeted AARE may act as an ATP-independent defense to prevent or attenuate protein aggregation in the major ROS-producing organelles.

Based on localization prediction, 70% of our selected plant species possess one AARE isoform that localizes to either plastids or to mitochondria. Whether dual targeting via ambiguous targeting also occurs in these species remains to be experimentally validated. Further, we do not exclude that the remaining species also have organellar AARE isoforms, because our predictions may be compromised by incomplete gene models. Such incomplete AARE gene models without a transit peptide were present in earlier genome annotations of *Arabidopsis* and *Physcomitrella*^{41,53}, whilst complete gene models with transit peptides were only introduced with later versions^{39,62}.

It is not yet clear how translation of both variants in *Arabidopsis* is regulated, but a recent study highlights the importance of alternative translation initiation in shaping different subcellular localizations or functions of proteoforms¹¹⁰. This mechanism is also present in *Physcomitrella*, where dual targeting of FtsZ isoforms to the cytoplasm and chloroplasts is enabled via alternative translation initiation¹¹¹. Thus, localization of *PpAARE1* to the cytoplasm is also possible from the longer splice variant. Alternative translation initiation of *AtAARE* is further evidenced by proteomics data (www.peptideatlas.org/builds/arabidopsis/)¹¹². Here, we found evidence for N-terminal acetylation of M⁵⁶ which is the initiator methionine of the short variant (PXD012708¹¹³).

A reporter fusion of the shorter *AtAARE* ORF was observed in the cytoplasm and in the nucleus²¹. We did not detect a nuclear localization of any AARE isoform. Using *LOCALIZER*⁶⁴ we identified an NLS in *AtAARE*, in *PpAARE1* and *PpAARE3*, but not in *PpAARE2*. In contrast, the human AARE homolog HsACPH does not have a predictable NLS, but nuclear import is mediated via interaction with XRCC1 under stress, where it acts in DNA-damage repair¹¹⁴. Similarly, a nuclear localization of AARE might also occur under stress *in planta*.

In *Physcomitrella*, AARE1 is the dominant exopeptidase, whereas AARE2 acts predominantly as endopeptidase, and the operation mode of AARE3 remains unresolved. Crystal structures from bacterial and archaeal AAREs revealed two possible entrances for substrates to the catalytic centers^{14,115} but the mode of substrate entry is not fully understood. Although the quaternary arrangements of subunits differ between species^{115,116}, the secondary structure arrangement is conserved across kingdoms and specific subunit interactions (multimerization) are likely a mechanism to mediate substrate specificity and modulate activity. This could be further used as a switch between endopeptidase and exopeptidase activity and additionally enable access of the catalytic center via structural re-arrangements. Accordingly, the interaction between the distinct *PpAARE* isoforms may modify substrate specificity and activity.

Our data indicate a partial compensation between *PpAARE1* and *PpAARE2*. Both single KO mutants are phenotypically inconspicuous under normal conditions, although a significant reduction in exopeptidase activity was observed in $\Delta PpAARE1$. *PpAARE2* had the strongest effect on the accumulation of oxidized proteins in gametophores on the single isoform KO level, whereas the double KO of *PpAARE1* and *PpAARE2* showed the most striking effect in all lines as accelerated transition from protonema to gametophores. This phenotype is similar to mutants with disturbed auxin transport¹¹⁷. However, colony growth in these mutants was reduced which is different from our double KO mutant (*PpAARE1/2*). Intriguingly, this double KO results in stunted gametophores and a reduced life span. This phenotype partially resembles a loss-of-function mutant of a central component of autophagy (*PpATG3*) in *Physcomitrella*¹¹⁸. In $\Delta PpATG3$, gametophores exhibit a reduced life span and colonies are smaller than in WT. In contrast, gametophore size was not affected. Further, photosynthetic capacity in $\Delta PpATG3$ was also reduced, an effect which is apparently not caused by

AARE depletion²¹ and *PpAARE* genes were not differentially expressed in $\Delta PpATG3$ ¹¹⁸. We conclude that the reduced life span observed in $\Delta PpAARE1/2$ and $\Delta PpAARE1/3/2$ is not due to an impaired autophagy system causing nitrogen starvation. This is in line with data which opposes autophagy at the onset of senescence in *Arabidopsis*¹¹⁹.

In mammals, elevated levels of oxidized proteins are associated with age-related pathologies, such as Alzheimer's disease, diabetes and different types of carcinomas¹²⁰. If proteolytic clearance fails, further accumulation of oxidized proteins causes protein aggregation, which is a hallmark of ageing in animals^{96,121,122}. A connection between protein oxidation and ageing was less well studied in plants. Plastid ROS levels increase during ageing⁹², which is in line with strong oxidation of plastid proteins in ageing leaves⁸⁶. Likewise, protein oxidation marks the developmental transition between vegetative growth and flowering in *Arabidopsis*⁸⁶. *Physcomitrella* mutants $\Delta PpAARE1/2$ and $\Delta PpAARE1/3/2$ showed accelerated developmental transition from protonema to gametophores, reduced life span and increased levels of oxidized proteins as signs of accelerated ageing. This is supported by the fact that gametophore tips, which is younger tissue, are viable longer than the older stems in both mutants. In the *Arabidopsis* AARE T-DNA mutants we found increased levels of oxidized proteins under normal cultivation conditions and an accelerated developmental transition, in this case premature bolting. These findings suggest an evolutionary conserved connection between protein oxidation and ageing.

We provide here a detailed analysis of AARE genes in the plant lineage and an in-depth analysis of AARE localization and function in the moss *Physcomitrella* and the annual angiosperm *Arabidopsis*. AARE loss-of-function mutants have not been described for any organism so far. We generated and analyzed such mutants and describe a connection between AARE function, aggregation of oxidized proteins and plant ageing, including accelerated developmental progression and reduced life span. Our findings complement similar findings in humans and animals where AARE malfunction is associated with protein aggregation and age-related pathologies.

To solidify the role of AARE in ageing in different life forms, particularly in plants with contrasting maximum life spans and in animals of different complexity, loss-of-function mutants should be established and analyzed in selected model species. Likewise, a deeper understanding of AARE function in human diseases is desirable. Together, such analyses may contribute to a unified concept of ageing in different life forms.

Methods

Cultivation of *Physcomitrella*. *Physcomitrella* WT (new species name: *Physcomitrium patens* (Hedw.) Mitt¹²³); ecotype "Gransden 2004" and AARE KO lines were cultivated in Knop medium¹²⁴ supplemented with microelements. Knop medium (pH 5.8) containing 250 mg/L KH_2PO_4 , 250 mg/L KCl, 250 mg/L $MgSO_4 \times 7 H_2O$, 1,000 mg/L $Ca(NO_3)_2 \times 4 H_2O$ and 12.5 mg/L $FeSO_4 \times 7 H_2O$ supplemented with 10 mL per litre of a microelement (ME) stock solution^{125,126} (309 mg/L H_3BO_3 , 845 mg/L $MnSO_4 \times 1 H_2O$, 431 mg/L $ZnSO_4 \times 7 H_2O$, 41.5 mg/L KI, 12.1 mg/L $Na_2MoO_4 \times 2 H_2O$, 1.25 mg/L $CoSO_4 \times 5 H_2O$, 1.46 mg/L $Co(NO_3)_2 \times 6 H_2O$). For cultivation on solid medium, 12 g/L Agar was added to the KnopME medium. Moss suspension cultures were disrupted weekly with an ULTRA-TURRAX (IKA) at 18,000 rpm for 90 s. If not indicated otherwise, moss was grown under standard light conditions (55 μ mol photons/m²s) at 22 °C in a 16 h/8 h light/dark cycle.

Hydroponic *Physcomitrella* gametophore cultures were assembled as described^{36,127}. Here, a thin layer of protonema from suspension was distributed on gauze mesh (PP, 250 m mesh, 215 m thread, Zitt Thoma GmbH, Freiburg, Germany) capped on a glass ring. The glass rings with protonema-covered mesh gauze were placed in Magenta® Vessels (Sigma-Aldrich, St. Louis, USA) and KnopME medium was added until the protonema-covered gauze mesh was moist. The medium was exchanged every 4 weeks. Gametophores were harvested after 12 weeks.

Gametophore colonies on Agar plates (KnopME) were generated by transplanting single gametophores to new plates. Plates were sealed with Parafilm®.

Generation of AARE knockout lines. Knockout constructs for each *PpAARE* gene were generated by amplifying genomic regions as homologous flanks. The PCR products were fused to a neomycin (*PpAARE1*), hygromycin (*PpAARE2*), and zeocin (*PpAARE3*) resistance cassettes, respectively, employing triple template PCR as described¹²⁸ with primer sequences listed in Supplementary Data S1 using the Q5 polymerase (New England Biolabs, Ipswich, USA). The knockout constructs were released from their vector backbones with XhoI (*PpAARE1*), BglIII (*PpAARE2*) and DraI (*PpAARE3*), respectively. Enzymes were purchased from Thermo Fisher Scientific. Digested plasmids were precipitated and sterilized prior to transfection using standard ethanol precipitation method¹²⁹. Transfection of *Physcomitrella* WT or KO (for consecutive knockouts) protoplasts was conducted via PEG-mediated procedure^{77,130}. The WT strain as well as the identified *PpAARE* KO lines are accessible via the International Moss Stock Center (IMSC, www.moss-stock-center.org). IMSC accession numbers for the mutants and WT are available in Supplementary Data S4.

Screening of plants surviving antibiotics selection was done by PCR. KO mutant plants surviving the antibiotics selection were checked for the presence of a genomic region which should be removed upon homologous recombination-based integration of the knockout construct (Fig. S4a). In case of the absence of this WT signal, plants were further checked for correct 5' and 3' integration of the respective knockout construct using primers listed in Supplementary Data S1.

Protonema growth and gametophore induction. Suspension cultures were started at the same day and disrupted weekly as described. Dry weight was measured in triplicates and suspension density was adjusted to 440 mg dry weight (DW) per litre (mg DW/L) as described¹³¹. Droplets of 15 μ L were distributed on solid medium (Knop ME, 0.02% glucose). Sealed plates were cultivated as described above. Three droplets each per line were distributed on one plate and all lines were grown on the same plate. 4 plates (12 colonies) were used per assay. Colony areas were measured with *ImageJ*. White pixels counted from binarized colony images were used as quantitative values. Gametophores were counted upon visibility of the first leafy structure on buds.

Generation of PpAARE-Citrine knock-in lines. Knock-in constructs to fuse the coding sequence of Citrine to the C-terminus of *PpAARE* isoforms via an 18 bp linker¹²⁸ at the endogenous genomic locus were cloned via Gibson assembly¹³². All necessary parts were amplified using primers listed in Supplementary Data S1. Additionally, XhoI (*PpAARE1*), Sall (*PpAARE2*), and BamHI (*PpAARE3*) restriction sites were added to the 5' and 3' ends of the respective knock-in construct. All parts were assembled into pJet1.2 vector backbone (Thermo Scientific) using the Gibson Assembly® Cloning Kit from New England Biolabs (Ipswich, Massachusetts, USA). Transfection of *Physcomitrella* WT protoplasts were conducted as described^{77,130} by co-transfecting a plasmid containing a neomycin phosphotransferase resistance (nptII) cassette as transient selection marker (pBSNNEV, Mueller et al.⁵⁷). The linearized plasmid and the co-transfection vector were purified and sterilized via ethanol precipitation¹²⁹ prior to transfection.

The presence of Citrine was checked with primers listed in Supplementary Data S1 and resulting positive lines were further checked for correct 5' and 3' integration by PCR using the Plant Phire Kit with primers listed in Supplementary Data S1. All identified fusion lines are available via the International Moss Stock Center (IMSC, www.moss-stock-center.org). IMSC accessions are listed in Supplementary Data S4.

qPCR analysis. The copy number of the integrated KO constructs was determined using a qPCR-based method⁷⁸. Genomic DNA was extracted from 100 mg frozen protonema using the GeneJET Plant Genomic DNA Purification Kit (Thermo Scientific, Waltham, USA). DNA concentrations were adjusted to 3 ng/ μ L for each sample and qPCR was performed with primers for the 5' and 3' flanks as well as with primers for the corresponding selection cassette. Additionally, primers for the single copy gene *CLF* (Pp3c22_2940V3) were used as internal control. Reference lines were WT as well as in-house lines with known single integrations of the used selection cassettes. Primers are listed in Supplementary Data S5. PCR reactions were done using 2x SensiFAST Mix (Bioline, London, UK) and analyzed in a Lightcycler 480 II (Roche, Basel, Schweiz).

cDNA preparation. RNA was extracted using the innuPREP Plant RNA Kit (Analytik Jena, Jena, Germany). The extracted RNA was treated with DNase I (Thermo Scientific) and subsequently reverse transcribed into cDNA using Superscript III Reverse Transcriptase (Life Technologies, Carlsbad, USA).

Fusion constructs for subcellular localization. All constructs were generated using Gibson assembly¹³² and integrated into a PpAct5:Linker:eGFP-MAV4 vector backbone⁷³. Integration of the different coding sequences was done in frame in front of the Linker:eGFP. All parts for the Gibson assembly (inserts and corresponding vector backbones) were amplified either with Phusion™ polymerase (Thermo Fisher Scientific) or with HiFi polymerase (PCR Biosystems Ltd) according to the manufacturer's instructions. The primers were designed to have a 25 bp overlap to the corresponding fragment to be fused with. All primers and combinations are listed in Supplementary Data S6. In the case of the N-terminal

difference of AtAARE (M1-A⁵⁵ of AT4G14570.1, gene model provided by TAIR (<https://www.arabidopsis.org/>)) the Actin5 promoter was replaced by the CaMV35S promoter¹³³ previously validated in *Physcomitrella*¹³⁴.

Cloned plasmids were purified using the PureYield™ Plasmid Midiprep kit (Promega, Wisconsin, USA) according to the manufacturer's instructions. The plasmids were purified and sterilized via ethanol precipitation¹²⁹.

Confocal microscopy. Confocal imaging was performed on transiently transfected live protoplasts using Leica TCS SP8 (Leica Microsystems, Wetzlar, Germany). Immediately before microscopy, MitoTracker™ Orange CMTMRos (Thermo Fisher Scientific) was added to protoplast suspensions to a final concentration of 100 nM. For all imaging experiments, an HC PL APO CS2 63x/1.40 OIL objective was used with a zoom factor of 4. The pinhole was set to 35.4 μm. For excitation, a WLL laser (70%) was used. In a sequential acquisition setup, eGFP and chlorophyll were excited with the same laser beam (488 nm, 2%) and their signals were detected simultaneously, whereas MitoTracker™ was excited with a different laser beam (550 nm, 2%) and its signal was detected separately. The detection ranges were specified as 502–546 nm for eGFP, 662–732 nm for chlorophyll, and 597–636 nm for MitoTracker™. The images were acquired as z-stacks with the number of optical sections varying with the protoplast size. The voxel sizes of the resulting z-stacks were 0.0903, 0.0903, 0.239 μm in the x-y-z order. For visual representation and analysis, single slices with the best signal-to-noise ratio were selected and extracted from each z-stack using Fiji software.

Cultivation of Arabidopsis. Seeds were surface-sterilized for 4 min in 80% ethanol and subsequently for 1 min in 100% ethanol. Seeds were placed on plates containing ½ MS supplemented with 1% (D +) sucrose and 0.8% Agar. Alternatively, seeds were directly placed on sterilized soil. Seeds were incubated at 8 °C for 2–4 days in the dark for stratification before placing them in growth chambers. Plants were further cultivated under short day conditions at 22 °C and 70 μmol photons/m²s in an 8 h/16 h light/dark cycle. For bolting assays, plants were placed in a phytochamber at 22 °C and 70 μmol photons/m²s in a 16 h/8 h light/dark cycle (long day condition). Rosette leaves and days since sowing were counted upon appearance of the shoot in the middle of the rosette.

Screening of Arabidopsis AARE mutants. *Arabidopsis thaliana* lines with T-DNA insertions in the At4G14570 locus were identified from the public T-DNA Express database at the SIGnAL website (Salk Institute Genomic Analysis Laboratory). Lines GK-456A10, SALK_080653C, SALK_071125C, and SALK_205137C, were obtained from the Nottingham Arabidopsis Stock Centre. Homozygous mutant alleles were verified by PCR using the following primers: forward LB GK 5'-ATATTGACCATCATACTCATTCG-3' and reverse GK-456 5'-CTTCAAAGAAACCAACTAG-3' for the GK-456A10 line, and forward LB-pROK 5'-CGGTGGACCGCTTGCTGCAACT-3' and reverse Salk_53 5'-TCTTAGCCGAATCAGTTCAGAG-3' for the SALK_080653C, SALK_071125C, and SALK_205137C lines. Identified homozygous mutant plants were back-crossed with Arabidopsis Col-0. The F2 generation was screened for homozygous mutant plants using the above listed primer sets to identify the mutant allele or substituting the forward primers with forward WT-GK-456 5'-AAGATGCTTTGCACTCTC TA-3' and forward WT-Salk 5'-ACTGCCATTATGATCCATTGCTCTC-3', to identify the GK and SALK lines WT alleles, respectively. RT-PCR was additionally performed to check for the presence of AtAARE transcripts using Taq polymerase on cDNA prepared as described above with primers At1-At4. All primer combinations are listed in Supplementary Data S4.

AARE exopeptidase activity. The enzyme activity assay according to¹⁷ was modified. Here, tissue (80–100 mg) was homogenized in liquid nitrogen and dissolved in 1 mL extraction buffer (50 mM PBS, 1 mM EDTA, 2 mM DTT). After centrifugation at 20,000 × g for 20 min at 4 °C, 300 μL supernatant was mixed with 700 μL reaction buffer (50 mM HEPES-KOH, pH 7.5 containing 1 mM AcAla-pNA (Bachem, Bubendorf, Switzerland) or 50 mM HEPES-KOH, pH 7.5, 10% DMSO containing 1 mM AcLeu-pNA (Bachem) and incubated at 37 °C for 30–120 min. The reaction was stopped by the addition of 500 μL 30% acetic acid. Absorbance was measured at 410 nm in a photometer. This approach was used to generate the data of Figs. 3b and S6a–d. Later the method was modified (Figs. 3g and S6e–g). Here, tissue was homogenized in liquid nitrogen and dissolved in 100 μL extraction buffer (50 mM PBS, 1 mM EDTA, 2 mM DTT) per 10 mg FW. After centrifugation at 20,000 × g for 20 min at 4 °C, 5 μL supernatant was mixed with 195 μL reaction buffer (50 mM HEPES-KOH, pH 7.5 containing 1 mM AcAla-pNA (Bachem, Bubendorf, Switzerland)) in a 96 well micro titer plate and incubated at 37 °C for 30–120 min. In the case of AcLeu-pNA as substrate, 50 mM HEPES-KOH, pH 7.5 with 10% DMSO containing 1 mM AcLeu-pNA (Bachem) was used as reaction buffer. Every biological sample was measured in three technical replicates. Absorbance was measured at 410 nm. Activity was calculated using a molar absorbance coefficient²¹ of 8.8 mM⁻¹cm⁻¹ and represents the release of pNA [μmol] per minute normalized to the total protein concentration of the sample. The protein concentration was determined using the A₂₈₀ method of a NanoDrop™ (Thermo Fisher Scientific) or with a Bradford assay¹³⁵.

Western blots. Western blots were performed as described⁷⁴ using the ECL Advance detection kit (GE Healthcare). The primary antibody against *A. thaliana* AARE was kindly provided by Dr. Yasuo Yamauchi¹⁷. The primary antibody was diluted 1:10,000 in TBST Buffer with 2% Blocking (GE Healthcare) and incubated on the membrane for 2 h. As secondary antibody anti-Guinea pig antibody, coupled to a horseradish peroxidase (Agrisera, AS 10 1496) diluted 1:10,000 in 2% TBST with 2% Blocking (GE Healthcare), was applied for 1 h.

Detection of oxidized proteins. Plant tissues were homogenized in liquid nitrogen and proteins were extracted in 50 mM PBS, 50 mM DTT, 1 mM EDTA. In all, 3–6 μg total protein was derivatized with DNP and subsequently detected with an anti-DNP antibody according to the manufacturer's instruction of the OxyBlot Protein Oxidation Detection Kit (S7150, Sigma-Aldrich). Equal amounts of the derivatized protein samples were employed as loading control on a separate SDS-gel and stained with Coomassie or silver staining.

Flow cytometry. Flow cytometry analysis was performed as described⁷⁹. Here, protonemata were chopped with a razor blade in a small petri dish (6 cm diameter) in 2 mL of DAPI-buffer containing 0.01 mg/L 4',6-Diamidin-2-phenylindol (DAPI), 1.07 g/L MgCl₂ × 6 H₂O, 5 g/L NaCl, 21.11 g/L Tris, 0.1% Triton, pH 7. The solution was filtered using 30 μm pore size filters and the fluorescence intensity was measured using a Cyflow®Space flow cytometry system (Partec, Munich, Germany).

Computational predictions. Predictions for the presence of cleavable targeting peptides were performed with TargetP2.0⁶³. Additional predictions of subcellular localizations were performed with LOCALIZER⁶⁴. The presence of peroxisomal targeting signals was predicted with PredPlantPTS^{66,67}. Prediction of protein domains was performed using InterProScan¹³⁶ and protein domain annotations according to PFAM¹³⁷ were used.

Co-Immunoprecipitation. Co-immunoprecipitation was performed using GFP-Trap Magnetic Particles M-270 (Chromotek, Planegg-Martinsried, Germany) as recommended by the manufacturer with modifications. In all, 300 mg protonema was homogenized in a 2 mL reaction tube using a tungsten and a glass bead. For each line three biological replicates were realized. The extraction buffer was chosen according to the manufacturer's recommendations for plant samples and contained 25 mM HEPES-KOH, pH 7.5, 2 mM EDTA, 100 mM NaCl, 200 nM DTT, 0.5% Triton X-100, 1% plant protease inhibitor cocktail (PPI, P9599, Sigma Aldrich). Ground plant material was dissolved in a final volume of 2 mL ice-cold extraction buffer and incubated for 10 min in a water quench ultrasonic device. Samples were centrifuged at 4 °C at 20,000 × g for 30 min. For each sample 25 μL magnetic particle slurry was washed with 500 μL extraction buffer. The sample supernatant was transferred to the cleaned beads and incubated, rotating for 1 h at 6 °C. Subsequently, beads were washed with 1 mL extraction buffer without Triton and PPI and again with 500 μL. Beads were then dissolved in 500 μL wash buffer (10 mM Tris-HCl, pH 7.5, 150 mM NaCl, 0.5 mM EDTA), transferred to a new reaction tube and washed again in 500 μL wash buffer. A RapiGest solution (0.2% in 50 mM Tris-HCl, pH 7.5; RapiGest SF Surfactant (Waters, Milford, MA, USA) was mixed 3:1 with 5 mM DTT in 50 mM Tris-HCl, pH 7.5. 30 μL of the resulting mixture was applied to each sample. Samples were incubated at 95 °C for 5 min under continuous shaking. Samples were cooled down to RT and 5 μL of a trypsin (V5117, Promega) solution (0.025 μg/μL in 50 mM Tris-HCl, pH 7.5) were added to each sample. Digestion on the beads was performed for 30 min at 32 °C under continuous shaking. Supernatants were transferred to new reaction tubes and the remaining beads were washed twice with 50 μL 5 mM Iodoacetamide solution (in 50 mM Tris-HCl, pH 7.5). The wash supernatants were combined with the trypsin-containing supernatant and incubated over night at 30 °C under continuous shaking. Acid-catalyzed cleavage of the RapiGest surfactant was performed as recommended by the manufacturer. Samples were purified using C18-STAGE-Tips as described¹³⁸ and eluted from the tip in 30% ACN in 0.1% FA.

Mass spectrometry measurement and data analysis. MS analysis was performed on an Orbitrap Q-Exactive Plus instrument (Thermo Fisher Scientific) coupled to an UltiMate 3000 RSLCnano system (Dionex LC Packings/Thermo Fisher Scientific) as described¹³⁹. Database search and label-free quantitation was performed using MaxQuant software V1.6.0.16¹⁴⁰. For each Co-IP a specific database was employed containing all V3.3 proteins of *Physcomitrella*³⁹ as well as the sequence of the respective fusion protein. Additionally, the contaminant list provided by the software was included. Decoys were generated on the fly by reverting the given protein sequences. Variable modifications were formation of pyro Glu (N-term Q, -17.026549 Da), oxidation (M, + 15.994915 Da), acetylation (N-term, + 42.010565 Da) and deamidation (N, + 0.984016 Da). Carbamido-methylation (C, + 57.021464 Da) was specified as fixed modification. Enzymatic specificity was set to tryptic with semi-specific free N-terminus. An FDR of 0.01 was set for protein identification. LFQ values¹⁴¹ were used as quantitative values. Interaction analysis was performed in Perseus V1.6.12.0¹⁴². Missing values were imputed from a normal distribution with a down-shift of 1.8 and distribution

width of 0.3. Interaction partners were accepted at an FDR of 0.01 and a p -value < 0.01.

Raw files of the test-IP measurements (Fig. S8e) were processed using Mascot Distiller V2.7.10 and searched against all *Physcomitrella* protein models V3.3³⁹ using Mascot Server V2.7.0 (Matrix Science). Processed mgf files from immunoprecipitation experiments targeting N-terminal arginylation (PXD003232^{36,143}) and the test-IPs were searched again against all *Physcomitrella* protein models V3.3³⁹ using Mascot Server V2.7.0 (Matrix Science). The precursor mass tolerance was 5 ppm and the fragment mass tolerance was 0.02 Da. Variable modifications were formation of pyro Glu (N-term Q, −17.026549 Da), oxidation (M, +15.994915 Da), acetylation (N-term, +42.010565 Da) and deamidation (N, +0.984016 Da). Carbamidomethylation (C, +57.021464 Da) was specified as fixed modification. Enzymatic specificity was set to tryptic with semi-specific free N-terminus. Search results were loaded in ScaffoldTM 5 (V5.0.1, Proteome Software) and proteins were accepted at an FDR = 1 and peptides at an FDR = 0.5. A table of identified proteins is accessible in Supplementary Data S7.

Multiple sequence alignment and phylogenetic reconstruction. Homologous protein sequences were aligned with UPP¹⁴⁴ (version 4.4.0) using default parameters and subsequently translated into a codon-aware CDS alignment with PAL2NAL¹⁴⁵ (version 1.4). Based on this multiple coding sequence alignment we reconstructed a maximum likelihood tree with RAxML¹⁴⁶ (version 8.2.12) using the GTRCAT model with 1000 rapid bootstrap samples. The tree was rooted at the split between animal and plant sequences and plotted in R¹⁴⁷ using the packages *ape*¹⁴⁸ and *ggtree*¹⁴⁹.

Statistics and reproducibility. Statistical differences in datasets were analyzed with one-way Anova with subsequent post-hoc test if different lines at same conditions were compared. Two-way Anova with subsequent post-hoc test was performed to analyze differences between lines at different conditions. Sample sizes of biological replicates are specified in the figure legends. Anova and post-hoc analysis was performed in R¹⁴⁷. Statistical significance was accepted at $*p < 0.05$, $**p < 0.01$, and $***p < 0.001$.

Reporting summary. Further information on research design is available in the Nature Portfolio Reporting Summary linked to this article.

Data availability

The authors confirm that all relevant data supporting the findings of this study are available within the paper and its supplementary files. The mass spectrometry proteomics data have been deposited at the ProteomeXchange Consortium via the PRIDE partner repository^{84,85} with the dataset identifier PXD033854 and 10.6019/PXD038742. Plant lines used in this study are available upon reasonable request from the corresponding author (R.R.) or via the International Moss Stock Center (IMSC, www.moss-stock-center.org). IMSC accessions are listed in Supplementary Data S4. Full Blot images for Fig. 6b and Fig. S3b are available in Fig. S10. Supplementary Data S8 contains all numeric source data used to generate the graphs and charts in this study. Plasmids generated in this study are available from the International Moss Stock Center IMSC (<https://www.moss-stock-center.org>) with the accession numbers P1519 (*PpAARE1* KO (pJet)), P1841 (*PpAARE2* KO (pJet)), P1520 (*PpAARE3* KO (pJet)), P1655 (*PpAARE1:Citrine* KI (pJet)), P1813 (*PpAARE2:Citrine* KI (pJet)), P1814 (*PpAARE3:Citrine* KI (pJet)), P1833 (*PpAARE1_1:eGFP* (pMAV4)), P1834 (*PpAARE1_2:eGFP* (pMAV4)), P1853 (*PpAARE1_Nt:eGFP* (pMAV4)), P1855 (*PpAARE3:eGFP* (pMAV4)), P1856 (*PpAARE3:eGFP* (pMAV4)), P1854 (*AtAARE_SV:eGFP* (pMAV4)), P1881 (*AtAARE_LV:eGFP* (pMAV4)) and P1862 (*AtAARE_Nt:eGFP* (pMAV4)).

Received: 11 August 2022; Accepted: 5 January 2023;

Published online: 17 January 2023

References

- Mittler, R., Zandalinas, S. I., Fichman, Y. & Van Breusegem, F. Reactive oxygen species signalling in plant stress responses. *Nat. Rev. Mol. Cell Biol.* **23**, 663–679 (2022).
- Tola, A. J., Jaballi, A. & Missihoun, T. D. Protein carbonylation: emerging roles in plant redox biology and future prospects. *Plants* **10**, 1451 (2021).
- Gratão, P. L., Polle, A., Lea, P. J. & Azevedo, R. A. Making the life of heavy metal-stressed plants a little easier. *Funct. Plant Biol.* **32**, 481–494 (2005).
- Smirnoff, N. Ascorbic acid: metabolism and functions of a multi-faceted molecule. *Curr. Opin. Plant Biol.* **3**, 229–235 (2000).
- Sharma, P., Jha, A. B., Dubey, R. S. & Pessarakli, M. Reactive oxygen species, oxidative damage, and antioxidative defense mechanism in plants under stressful conditions. *J. Bot.* **2012**, 217037 (2012).
- Müller-Schüssele, S. J. et al. Chloroplasts require glutathione reductase to balance reactive oxygen species and maintain efficient photosynthesis. *Plant J.* **103**, 1140–1154 (2020).
- Soares, C., Carvalho, M. E., Azevedo, R. A. & Fidalgo, F. Plants facing oxidative challenges—a little help from the antioxidant networks. *Environ. Exp. Bot.* **161**, 4–25 (2019).
- Parsell, D. A., Kowal, A. S., Singer, M. A. & Lindquist, S. Protein disaggregation mediated by heat-shock protein Hsp104. *Nature* **372**, 475–478 (1994).
- Queitsch, C., Hong, S. W., Vierling, E. & Lindquist, S. Heat shock protein 101 plays a crucial role in thermotolerance in *Arabidopsis*. *Plant Cell* **12**, 479–492 (2000).
- Mogk, A., Bukau, B. & Kampinga, H. H. Cellular handling of protein aggregates by disaggregation machines. *Mol. Cell* **69**, 214–226 (2018).
- Møller, I. M., Jensen, P. E. & Hansson, A. Oxidative modifications to cellular components in plants. *Annu. Rev. Plant Biol.* **58**, 459–481 (2007).
- Ciacka, K., Tyminiński, M., Gniazdowska, A. & Krasuska, U. Carbonylation of proteins—an element of plant ageing. *Planta* **252**, 12 (2020).
- Farooq, M. A. et al. Acquiring control: the evolution of ROS-Induced oxidative stress and redox signaling pathways in plant stress responses. *Plant Physiol. Biochem.* **141**, 353–369 (2019).
- Bartlam, M. et al. Crystal structure of an acylpeptide hydrolase/esterase from *Aeropyrum pernix* K1. *Structure* **12**, 1481–1488 (2004).
- Brunialti, E. A., Gatti-Lafranconi, P. & Lotti, M. Promiscuity, stability and cold adaptation of a newly isolated acylaminoacyl peptidase. *Biochimie* **93**, 1543–1554 (2011).
- Tsunasawa, S., Narita, K. & Ogata, K. Purification and properties of acylamino acid-releasing enzyme from rat liver. *J. Biochem.* **77**, 89–102 (1975).
- Yamauchi, Y., Ejiri, Y., Toyoda, Y. & Tanaka, K. Identification and biochemical characterization of plant acylamino acid-releasing enzyme. *J. Biochem.* **134**, 251–257 (2003).
- Rawlings, N. D. et al. The MEROPS database of proteolytic enzymes, their substrates and inhibitors in 2017 and a comparison with peptidases in the PANTHER database. *Nucleic Acids Res.* **46**, D624–D632 (2018).
- Fujino, T. et al. Identification of the cleavage sites of oxidized protein that are susceptible to oxidized protein hydrolase (OPH) in the primary and tertiary structures of the protein. *J. Biochem.* **127**, 1087–1093 (2000).
- Shimizu, K. et al. Overexpression of oxidized protein hydrolase protects COS-7 cells from oxidative stress-induced inhibition of cell growth and survival. *Biochem. Biophys. Res. Commun.* **304**, 766–771 (2003).
- Nakai, A., Yamauchi, Y., Sumi, S. & Tanaka, K. Role of acylamino acid-releasing enzyme/oxidized protein hydrolase in sustaining homeostasis of the cytoplasmic antioxidative system. *Planta* **236**, 427–436 (2012).
- Gogliettino, M. et al. A novel class of bifunctional acylpeptide hydrolases—potential role in the antioxidant defense systems of the Antarctic fish *Trematomus bernacchii*. *FEBS J.* **281**, 401–415 (2014).
- Kiss, A. L. et al. The acylaminoacyl peptidase from *Aeropyrum pernix* K1 thought to be an exopeptidase displays endopeptidase activity. *J. Mol. Biol.* **368**, 509–520 (2007).
- Szeltner, Z. et al. Characterization of a novel acylaminoacyl peptidase with hexameric structure and endopeptidase activity. *Biochim. Biophys. Acta (BBA)-Proteins Proteom.* **1794**, 1204–1210 (2009).
- Gogliettino, M. et al. Identification and characterisation of a novel acylpeptide hydrolase from *Sulfolobus solfataricus*: structural and functional insights. *PLoS ONE* **7**, e37921 (2012).
- Scaloni, A. et al. Deficiency of acylpeptide hydrolase in small-cell lung carcinoma cell lines. *J. Lab. Clin. Med.* **120**, 546–552 (1992).
- Riccio, A. et al. A new APEH cluster with antioxidant functions in the antarctic hemoglobinless icefish *Chionodraco hamatus*. *PLoS ONE* **10**, e0125594 (2015).
- Gogliettino, M. et al. Selective inhibition of acylpeptide hydrolase in SAOS-2 osteosarcoma cells: is this enzyme a viable anticancer target? *Mol. Biol. Rep.* **48**, 1505–1519 (2021).
- Tangri, A. et al. Deubiquitinase UCHL1 maintains protein homeostasis through the PSMA7–APEH–Proteasome axis in high-grade serous ovarian carcinoma. *Mol. Cancer Res.* **19**, 1168–1181 (2021).
- Palumbo, R. et al. APEH inhibition affects osteosarcoma cell viability via downregulation of the proteasome. *Int. J. Mol. Sci.* **17**, 1614 (2016).
- Shimizu, K., Kiuchi, Y., Ando, K., Hayakawa, M. & Kikugawa, K. Coordination of oxidized protein hydrolase and the proteasome in the clearance of cytotoxic denatured proteins. *Biochem. Biophys. Res. Commun.* **324**, 140–146 (2004).
- Palmieri, G. et al. Acylpeptide hydrolase inhibition as targeted strategy to induce proteasomal down-regulation. *PLoS ONE* **6**, e25888 (2011).
- Bergamo, P. et al. RedOx status, proteasome and APEH: Insights into anticancer mechanisms of t10, c12-conjugated linoleic acid isomer on A375 melanoma cells. *PLoS ONE* **8**, e80900 (2013).

34. Yamin, R., Zhao, C., O'Connor, P. B., McKee, A. C. & Abraham, C. R. Acyl peptide hydrolase degrades monomeric and oligomeric amyloid-beta peptide. *Mol. Neurodegener.* **4**, 33 (2009).
35. Bachovchin, D. A. et al. A high-throughput, multiplexed assay for superfamily-wide profiling of enzyme activity. *Nat. Chem. Biol.* **10**, 656–663 (2014).
36. Hoernstein, S. N. W. et al. Identification of targets and interaction partners of arginyl-tRNA protein transferase in the moss *Physcomitrella patens*. *Mol. Cell. Proteom.* **15**, 1808–1822 (2016).
37. Schuessele, C. et al. Spatio-temporal patterning of arginyl-tRNA protein transferase (ATE) contributes to gametophytic development in a moss. *N. Phytologist* **209**, 1014–1027 (2016).
38. Varshavsky, A. N-degron and C-degron pathways of protein degradation. *Proc. Natl Acad. Sci. USA* **116**, 358–366 (2019).
39. Lang, D. et al. The *Physcomitrella patens* chromosome-scale assembly reveals moss genome structure and evolution. *Plant J.* **93**, 515–533 (2018).
40. Chen, F., Mackey, A. J., Stoeckert, C. J. Jr & Roos, D. S. OrthoMCL-DB: querying a comprehensive multi-species collection of ortholog groups. *Nucleic Acids Res.* **34**, D363–D368 (2006).
41. Zimmer, A. D. et al. Reannotation and extended community resources for the genome of the non-seed plant *Physcomitrella patens* provide insights into the evolution of plant gene structures and functions. *BMC Genomics* **14**, 498 (2013).
42. Fernandez-Pozo, N. et al. PEATmoss (*Physcomitrella* Expression Atlas Tool): a unified gene expression atlas for the model plant *Physcomitrella patens*. *Plant J.* **102**, 165–177 (2020).
43. Mergner, J. et al. Mass-spectrometry-based draft of the *Arabidopsis* proteome. *Nature* **579**, 409–414 (2020).
44. Altschul, S. F. et al. Gapped BLAST and PSI-BLAST: a new generation of protein database search programs. *Nucleic Acids Res.* **25**, 3389–3402 (1997).
45. Merchant, S. S. et al. The *Chlamydomonas* genome reveals the evolution of key animal and plant functions. *Science* **318**, 245–250 (2007).
46. Bowman, J. L. et al. Insights into land plant evolution garnered from the *Marchantia polymorpha* genome. *Cell* **171**, 287–304 (2017).
47. Banks, J. A. et al. The *Selaginella* genome identifies genetic changes associated with the evolution of vascular plants. *Science* **332**, 960–963 (2011).
48. Ouyang, S. et al. The TIGR rice genome annotation resource: improvements and new features. *Nucleic Acids Res.* **35**, D883–D887 (2007).
49. Tuskan, G. A. et al. The genome of black cottonwood, *Populus trichocarpa* (Torr. & Gray). *Science* **313**, 1596–1604 (2006).
50. Hori, K. et al. *Klebsormidium flaccidum* genome reveals primary factors for plant terrestrial adaptation. *Nat. Commun.* **5**, 3978 (2014).
51. Kirbis, A. et al. Transcriptional landscapes of divergent sporophyte development in two mosses, *Physcomitrium* (*Physcomitrella*) *patens* and *Funaria hygrometrica*. *Front. Plant Sci.* **11**, 747 (2020).
52. Ostendorf, A. K. et al. Polyploidization within the Funariaceae – a key principle behind speciation, sporophyte reduction and the high variance of spore diameters? *Bryophyt. Divers. Evol.* **43**, 164–179 (2021).
53. Lamesch, P. et al. The *Arabidopsis* Information Resource (TAIR): improved gene annotation and new tools. *Nucleic Acids Res.* **40**, D1202–D1210 (2012).
54. Rawlings, N. D., Polgar, L. & Barrett, A. J. A new family of serine-type peptidases related to prolyl oligopeptidase. *Biochem. J.* **279**, 907–908 (1991).
55. Polgar, L. The prolyl oligopeptidase family. *Cell. Mol. Life Sci.* **59**, 349–362 (2002).
56. Perroud, P. F. et al. The *Physcomitrella patens* gene atlas project: large-scale RNA-seq based expression data. *Plant J.* **95**, 168–182 (2018).
57. Mueller, S. J. et al. Quantitative analysis of the mitochondrial and plastid proteomes of the moss *Physcomitrella patens* reveals protein macrocompartmentation and microcompartmentation. *Plant Physiol.* **164**, 2081–2095 (2014).
58. Fesenko, I. A. et al. Specific pools of endogenous peptides are present in gametophore, protonema, and protoplast cells of the moss *Physcomitrella patens*. *BMC Plant Biol.* **15**, 87 (2015).
59. Fesenko, I. et al. The *Physcomitrella patens* chloroplast proteome changes in response to protoplastation. *Front. Plant Sci.* **7**, 1661 (2016).
60. Liu, H. et al. The emergence and evolution of intron-poor and intronless genes in intron-rich plant gene families. *Plant J.* **105**, 1072–1082 (2021).
61. Beike, A. K. et al. Insights from the cold transcriptome of *Physcomitrella patens*: global specialization pattern of conserved transcriptional regulators and identification of orphan genes involved in cold acclimation. *New Phytol.* **205**, 869–881 (2015).
62. Cheng, C. Y. et al. Araport11: a complete reannotation of the *Arabidopsis thaliana* reference genome. *Plant J.* **89**, 789–804 (2017).
63. Armenteros, J. J. A. et al. Detecting sequence signals in targeting peptides using deep learning. *Life Sci. Alliance* **2**, e201900429 (2019).
64. Sperschneider, J. et al. LOCALIZER: subcellular localization prediction of both plant and effector proteins in the plant cell. *Sci. Rep.* **7**, 44598 (2017).
65. Waszczak, C., Carmody, M. & Kangasjärvi, J. Reactive oxygen species in plant signaling. *Annu. Rev. Plant Biol.* **69**, 209–236 (2018).
66. Lingner, T. et al. Identification of novel plant peroxisomal targeting signals by a combination of machine learning methods and in vivo subcellular targeting analyses. *Plant Cell* **23**, 1556–1572 (2011).
67. Reumann, S., Buchwald, D. & Lingner, T. PredPlantPTS1: a web server for the prediction of plant peroxisomal proteins. *Front. Plant Sci.* **3**, 194 (2012).
68. Gould, S. J., Keller, G. A., Hosken, N., Wilkinson, J. & Subramani, S. A conserved tripeptide sorts proteins to peroxisomes. *J. Cell Biol.* **108**, 1657–1664 (1989).
69. Wang, J., Wang, Y., Gao, C., Jiang, L. & Guo, D. PPero, a computational model for plant PTS1 type peroxisomal protein prediction. *PLoS ONE* **12**, e0168912 (2017).
70. Petriv, I., Tang, L., Titorenko, V. I. & Rachubinski, R. A. A new definition for the consensus sequence of the peroxisome targeting signal type 2. *J. Mol. Biol.* **341**, 119–134 (2004).
71. Reumann, S. Specification of the peroxisome targeting signals type 1 and type 2 of plant peroxisomes by bioinformatics analyses. *Plant Physiol.* **135**, 783–800 (2004).
72. Weise, A. et al. Use of *Physcomitrella patens* *actin* 5' regions for high transgene expression: importance of 5' introns. *Appl. Microbiol. Biotechnol.* **70**, 337–345 (2006).
73. Özdemir, B. et al. Cytological analysis and structural quantification of FtsZ1-2 and FtsZ2-1 network characteristics in *Physcomitrella patens*. *Sci. Rep.* **8**, 11165 (2018).
74. Lang, E. G. E. et al. Simultaneous isolation of pure and intact chloroplasts and mitochondria from moss as the basis for sub-cellular proteomics. *Plant Cell Rep.* **30**, 205–215 (2011).
75. Fuss, J., Liegmann, O., Krause, K. & Rensing, S. A. Green targeting predictor and ambiguous targeting predictor 2: the pitfalls of plant protein targeting prediction and of transient protein expression in heterologous systems. *New Phytol.* **200**, 1022–1033 (2013).
76. Orr, M. W., Mao, Y., Storz, G. & Qian, S. B. Alternative ORFs and small ORFs: shedding light on the dark proteome. *Nucleic Acids Res.* **48**, 1029–1042 (2020).
77. Hohe, A. et al. An improved and highly standardised transformation procedure allows efficient production of single and multiple targeted gene-knockouts in a moss, *Physcomitrella patens*. *Curr. Genet.* **44**, 339–347 (2004).
78. Noy-Malka et al. A single CMT methyltransferase homolog is involved in CHG DNA methylation and development of *Physcomitrella patens*. *Plant Mol. Biol.* **84**, 719–735 (2014).
79. Heck, M. A. et al. Axenic in vitro cultivation of 19 peat moss (*Sphagnum* L.) species as a resource for basic biology, biotechnology, and paludiculture. *New Phytol.* **229**, 861–876 (2021).
80. Kamisugi, Y. et al. The mechanism of gene targeting in *Physcomitrella patens*: homologous recombination, concatenation and multiple integration. *Nucleic Acids Res.* **34**, 6205–6214 (2006).
81. Rempfer, C. et al. Autopolyploidization affects transcript patterns and gene targeting frequencies in *Physcomitrella*. *Plant Cell Rep.* **41**, 153–173 (2022).
82. Lorenz, S., Tintelnot, S., Reski, R. & Decker, E. L. Cyclin D-knockout uncouples developmental progression from sugar availability. *Plant Mol. Biol.* **53**, 227–236 (2003).
83. Dalle-Donne, I. et al. Protein carbonylation: 2, 4-dinitrophenylhydrazine reacts with both aldehydes/ketones and sulfenic acids. *Free Radic. Biol. Med.* **46**, 1411–1419 (2009).
84. Deutsch, E. W. et al. The ProteomeXchange consortium in 2020: enabling 'big data' approaches in proteomics. *Nucleic Acids Res.* **48**, D1145–D1152 (2020).
85. Perez-Riverol, Y. et al. The PRIDE database resources in 2022: a hub for mass spectrometry-based proteomics evidences. *Nucleic Acids Res.* **50**, D543–D552 (2022).
86. Johansson, E., Olsson, O. & Nyström, T. Progression and specificity of protein oxidation in the life cycle of *Arabidopsis thaliana*. *J. Biol. Chem.* **279**, 22204–22208 (2004).
87. Harman, D. Aging: A theory based on free radical and radiation chemistry. *J. Gerontol.* **11**, 298–300 (1956).
88. Harman, D. The biologic clock: the mitochondria? *J. Am. Geriatr. Soc.* **20**, 145–147 (1972).
89. Giorgi, C. et al. Mitochondria and reactive oxygen species in aging and age-related diseases. *Int. Rev. Cell Mol. Biol.* **340**, 209–344 (2018).
90. Mao, C. et al. Nitric oxide regulates seedling growth and mitochondrial responses in aged oat seeds. *Int. J. Mol. Sci.* **19**, 1052 (2018).
91. Ratajczak, E., Małecka, A., Ciereszko, I. & Staszak, A. M. Mitochondria are important determinants of the aging of seeds. *Int. J. Mol. Sci.* **20**, 1568 (2019).
92. Munné-Bosch, S. & Alegre, L. Plant aging increases oxidative stress in chloroplasts. *Planta* **214**, 608–615 (2002).
93. Noctor, G., Veljovic-Jovanovic, S., Driscoll, S., Novitskaya, L. & Foyer, C. H. Drought and oxidative load in the leaves of C3 plants: a predominant role for photorespiration? *Ann. Bot.* **89**, 841–850 (2002).

94. Foyer, C. H. & Noctor, G. Redox sensing and signalling associated with reactive oxygen in chloroplasts, peroxisomes and mitochondria. *Physiol. Plant.* **119**, 355–364 (2003).
95. Sohal, R. S. & Weindruch, R. Oxidative stress, caloric restriction, and aging. *Science* **273**, 59–63 (1996).
96. López-Otin, C., Blasco, M. A., Partridge, L., Serrano, M. & Kroemer, G. The hallmarks of aging. *Cell* **153**, 1194–1217 (2013).
97. Senthilkumar, R., Reddy, P. N. & Sharma, K. K. Studies on trypsin-modified bovine and human lens acylpeptide hydrolase. *Exp. Eye Res.* **72**, 301–310 (2001).
98. Palmieri, G. et al. Low erythrocyte levels of proteasome and acyl-peptide hydrolase (APEH) activities in Alzheimer's disease: a sign of defective proteostasis? *J. Alzheimer's Dis.* **60**, 1097–1106 (2017).
99. Marshall, I. et al. Analyzing the activity and expression of acyl peptide enzyme hydrolase (APEH) in the blood serum of patients with type II diabetes. *Bios* **90**, 70–78 (2019).
100. Resemann, H. C. et al. Convergence of sphingolipid desaturation across over 500 million years of plant evolution. *Nat. Plants* **7**, 219–232 (2021).
101. Zybailov, B. et al. Sorting signals, N-terminal modifications, and abundance of the chloroplast proteome. *PLoS ONE* **3**, e1994 (2008).
102. Rugen, N. et al. Protein interaction patterns in *Arabidopsis thaliana* leaf mitochondria change in dependence to light. *Biochim. Biophys. Acta (BBA)-Bioenerg.* **1862**, 148443 (2021).
103. Maxwell, D. P., Wang, Y. & McIntosh, L. The alternative oxidase lowers mitochondrial reactive oxygen production in plant cells. *Proc. Natl Acad. Sci. USA* **96**, 8271–8276 (1999).
104. Møller, I. M. Plant mitochondria and oxidative stress: electron transport, NADPH turnover, and metabolism of reactive oxygen species. *Annu. Rev. Plant Biol.* **52**, 561–591 (2001).
105. Smakowska, E., Czarna, M. & Janska, H. Mitochondrial ATP-dependent proteases in protection against accumulation of carbonylated proteins. *Mitochondrion* **19**, 245–251 (2014).
106. Al-Khatib, K. & Paulsen, G. M. Enhancement of thermal injury to photosynthesis in wheat plants and thylakoids by high light intensity. *Plant Physiol.* **90**, 1041–1048 (1989).
107. Wang, Q. L., Chen, J. H., He, N. Y. & Guo, F. Q. Metabolic reprogramming in chloroplasts under heat stress in plants. *Int. J. Mol. Sci.* **19**, 849 (2018).
108. Sweetlove, L. J. et al. The impact of oxidative stress on *Arabidopsis* mitochondria. *Plant J.* **32**, 891–904 (2002).
109. Tiwari, B. S., Belenghi, B. & Levine, A. Oxidative stress increased respiration and generation of reactive oxygen species, resulting in ATP depletion, opening of mitochondrial permeability transition, and programmed cell death. *Plant Physiol.* **128**, 1271–1281 (2002).
110. Willems, P., Ndah, E., Jonckheere, V., van Breusegem, F. & van Damme, P. To new beginnings: riboproteomics discovery of N-terminal proteoforms in *Arabidopsis thaliana*. *Front. Plant Sci.* **12**, 778804 (2021).
111. Kiessling, J. et al. Dual targeting of plastid division protein FtsZ to chloroplasts and the cytoplasm. *EMBO Rep.* **5**, 889–894 (2004).
112. van Wijk, K. J. et al. The *Arabidopsis* PeptideAtlas: Harnessing worldwide proteomics data to create a comprehensive community proteomics resource. *Plant Cell* **33**, 3421–3453 (2021).
113. Zhang, H. et al. *Arabidopsis* proteome and the mass spectral assay library. *Sci. Data* **6**, 278 (2019).
114. Zeng, Z. et al. Acylpeptide hydrolase is a component of the cellular response to DNA damage. *DNA Repair* **58**, 52–61 (2017).
115. Brocca, S. et al. A bacterial acyl aminoacyl peptidase couples flexibility and stability as a result of cold adaptation. *FEBS J.* **283**, 4310–4324 (2016).
116. Menyhárd, D. K. et al. A self-compartmentalizing hexamer serine protease from *Pyrococcus horikoshii*: substrate selection achieved through multimerization. *J. Biol. Chem.* **288**, 17884–17894 (2013).
117. Viaene, T. et al. Directional auxin transport mechanisms in early diverging land plants. *Curr. Biol.* **24**, 2786–2791 (2014).
118. Chen, Z. et al. Comprehensive analysis of the *Ppatg3* mutant reveals that autophagy plays important roles in gametophore senescence in *Physcomitrella patens*. *BMC Plant Biol.* **20**, 440 (2020).
119. Jia, M. et al. Noncanonical ATG8–ABS3 interaction controls senescence in plants. *Nat. Plants* **5**, 212–224 (2019).
120. Dalle-Donne, I., Giustarini, D., Colombo, R., Rossi, R. & Milzani, A. Protein carbonylation in human diseases. *Trends Mol. Med.* **9**, 169–176 (2003).
121. Hipp, M. S., Kasturi, P. & Hartl, F. U. The proteostasis network and its decline in ageing. *Nat. Rev. Mol. Cell Biol.* **20**, 421–435 (2019).
122. Chen, Y. R., et al. Tissue-specific landscape of protein aggregation and quality control in an aging vertebrate. Preprint at: <https://doi.org/10.1101/2022.02.26.482120> (2022).
123. Medina, R. et al. Phylogenomic delineation of *Physcomitrium* (Bryophyta: Funariaceae) based on targeted sequencing of nuclear exons and their flanking regions rejects the retention of *Physcomitrella*, *Physcomitridium* and *Aphanorhagma*. *J. Syst. Evol.* **57**, 404–417 (2019).
124. Reski, R. & Abel, W. O. Induction of budding on chloronemata and caulonemata of the moss, *Physcomitrella patens*, using isopentenyladenine. *Planta* **165**, 354–358 (1985).
125. Egner, T. et al. High frequency of phenotypic deviations in *Physcomitrella patens* plants transformed with a gene-disruption library. *BMC Plant Biol.* **2**, 6 (2002).
126. Schween, G., Hohe, A., Koprivova, A. & Reski, R. Effects of nutrients, cell density and culture techniques on protoplast regeneration and early protonema development in a moss, *Physcomitrella patens*. *J. Plant Physiol.* **160**, 209–212 (2003).
127. Erxleben, A., Gessler, A., Vervliet-Scheebaum, M. & Reski, R. Metabolite profiling of the moss *Physcomitrella patens* reveals evolutionary conservation of osmoprotective substances. *Plant Cell Rep.* **31**, 427–436 (2012).
128. Tian, G. W. et al. High-throughput fluorescent tagging of full-length *Arabidopsis* gene products in planta. *Plant Physiol.* **135**, 25–38 (2004).
129. Sambrook, J. & Russell, D. W. Standard ethanol precipitation of DNA in microcentrifuge tubes. *Cold Spring Harb. Protoc.* **2006**, pdb-prot4456 (2006).
130. Hohe, A. & Reski, R. Optimisation of a bioreactor culture of the moss *Physcomitrella patens* for mass production of protoplasts. *Plant Sci.* **163**, 69–74 (2002).
131. Decker, E. L. et al. Strigolactone biosynthesis is evolutionarily conserved, regulated by phosphate starvation and contributes to resistance against phytopathogenic fungi in a moss, *Physcomitrella patens*. *New Phytol.* **216**, 455–468 (2017).
132. Gibson, D. G. et al. Enzymatic assembly of DNA molecules up to several hundred kilobases. *Nat. Methods* **6**, 343–345 (2009).
133. Amack, S. C. & Antunes, M. S. CaMV35S promoter—a plant biology and biotechnology workhorse in the era of synthetic biology. *Curr. Plant Biol.* **24**, 100179 (2020).
134. Horstmann, V., Huether, C. M., Jost, W., Reski, R. & Decker, E. L. Quantitative promoter analysis in *Physcomitrella patens*: a set of plant vectors activating gene expression within three orders of magnitude. *BMC Biotechnol.* **4**, 13 (2004).
135. Bradford, M. M. A rapid and sensitive method for the quantitation of microgram quantities of protein utilizing the principle of protein-dye binding. *Anal. Biochem.* **72**, 248–254 (1976).
136. Blum, M. et al. The InterPro protein families and domains database: 20 years on. *Nucleic Acids Res.* **49**, D344–D354 (2021).
137. Mistry, J. et al. Pfam: The protein families database in 2021. *Nucleic Acids Res.* **49**, D412–D419 (2021).
138. Hoernstein, S. N. W. et al. Host cell proteome of *Physcomitrella patens* harbors proteases and protease inhibitors under bioproduction conditions. *J. Proteome Res.* **17**, 3749–3760 (2018).
139. Top, O. et al. Expression of a human cDNA in moss results in spliced mRNAs and fragmentary protein isoforms. *Commun. Biol.* **4**, 964 (2021).
140. Cox, J. & Mann, M. MaxQuant enables high peptide identification rates, individualized ppb-range mass accuracies and proteome-wide protein quantification. *Nat. Biotechnol.* **26**, 1367–1372 (2008).
141. Cox, J. et al. Accurate proteome-wide label-free quantification by delayed normalization and maximal peptide ratio extraction, termed MaxLFQ. *Mol. Cell. Proteom.* **13**, 2513–2526 (2014).
142. Tyanova, S. et al. The Perseus computational platform for comprehensive analysis of (pro)teomics data. *Nat. Methods* **13**, 731–740 (2016).
143. Hoernstein, S. N. W. et al. Identification of N-terminally arginylated proteins from the moss *Physcomitrella patens*. <https://doi.org/10.6019/PXD003232> (2016).
144. Nguyen, N. D., Mirarab, S., Kumar, K. & Warnor, T. Ultra-large alignments using phylogeny-aware profiles. *Genome Biol.* **16**, 124 (2015).
145. Suyama, M., Torrents, D. & Bork, P. PAL2NAL: robust conversion of protein sequence alignments into the corresponding codon alignments. *Nucleic Acids Res.* **34**, W609–W612 (2006).
146. Stamatakis, A. RAxML version 8: a tool for phylogenetic analysis and post-analysis of large phylogenies. *Bioinformatics* **30**, 1312–1313 (2014).
147. R Core Team. *R: A Language And Environment For Statistical Computing* (R Foundation for Statistical Computing, 2022).
148. Paradis, E. & Schliep, K. ape 5.0: an environment for modern phylogenetics and evolutionary analyses in R. *Bioinformatics* **35**, 526–528 (2018).
149. Yu, G., Smith, D., Zhu, H., Guan, Y. & Lam, T. T. gtree: an R package for visualization and annotation of phylogenetic trees with their covariates and other associated data. *Methods Ecol. Evol.* **8**, 28–36 (2017).

Acknowledgements

We thank Christine Glockner, Agnes Novakovic and Eija Schulze for expert technical assistance and Anne Katrin Prowse for language editing. Support with the *Arabidopsis* assays from Dr. Philipp Schwenk is gratefully acknowledged. We thank Prof. Dr. Bettina Warscheid for the possibility to use the QExactive Plus instrument and Prof. Dr. Yasuo Yamauchi for the primary antibody against *A. thaliana* AARE. We gratefully acknowledge funding by the Deutsche Forschungsgemeinschaft (DFG, German Research

Foundation) under Germany's Excellence Strategy EXC-2189 (CIBSS to R.R.) and by the Wissenschaftliche Gesellschaft Freiburg.

Author contributions

S.N.W.H. designed research, performed experiments, analyzed data, and wrote the manuscript. B.Ö. and N.v.G. analyzed data and helped writing the manuscript. A.A.M. analyzed data. B.R.v.B., L.N., J.S.F., R.K., S.G., T.W., and F.S. performed experiments. M.R.F. and S.J.M.S. designed research and helped writing the manuscript. R.R. designed and supervised research, acquired funding, and wrote the manuscript. All authors approved the final version of the manuscript.

Funding

Open Access funding enabled and organized by Projekt DEAL.

Competing interests

The authors declare no competing interests.

Additional information

Supplementary information The online version contains supplementary material available at <https://doi.org/10.1038/s42003-023-04428-7>.

Correspondence and requests for materials should be addressed to Ralf Reski.

Peer review information *Communications Biology* thanks Ennio Cocca and the other, anonymous, reviewers for their contribution to the peer review of this work. Primary Handling Editor: Zhijuan Qiu. Peer reviewer reports are available.

Reprints and permission information is available at <http://www.nature.com/reprints>

Publisher's note Springer Nature remains neutral with regard to jurisdictional claims in published maps and institutional affiliations.



Open Access This article is licensed under a Creative Commons Attribution 4.0 International License, which permits use, sharing, adaptation, distribution and reproduction in any medium or format, as long as you give appropriate credit to the original author(s) and the source, provide a link to the Creative Commons license, and indicate if changes were made. The images or other third party material in this article are included in the article's Creative Commons license, unless indicated otherwise in a credit line to the material. If material is not included in the article's Creative Commons license and your intended use is not permitted by statutory regulation or exceeds the permitted use, you will need to obtain permission directly from the copyright holder. To view a copy of this license, visit <http://creativecommons.org/licenses/by/4.0/>.

© The Author(s) 2023